

Root hair developmental regulators orchestrate drought triggered microbiome changes and the interaction with beneficial Rhizobiaceae

Received: 4 January 2024

Accepted: 7 November 2024

Published online: 20 November 2024

 Check for updatesZhenghong Wang^{1,3}, Zewen Li^{1,3}, Yujie Zhang¹, Jingye Liao¹, Kaixiang Guan¹,
Jingxuan Zhai¹, Pengfei Meng¹, Xianli Tang¹, Tao Dong² & Yi Song^{1,2} 

Drought is one of the most serious abiotic stresses, and emerging evidence suggest plant microbiome affects plant drought tolerance. However, there is a lack of genetic evidence regarding whether and how plants orchestrate the dynamic assembly of the microbiome upon drought. By utilizing mutants with enhanced or decreased root hair densities, we find that root hair regulators also affect drought induced root microbiome changes. Rhizobiaceae is a key biomarker taxa affected by root hair related mutants. We isolated and sequenced 1479 root associated microbes, and confirmed that several *Rhizobium* strains presented stress-alleviating activities. Metagenome, root transcriptome and root metabolome studies further reveal the multi-omic changes upon drought stress. We knocked out an ornithine cyclodeaminase (*ocd*) gene in *Rhizobium* sp. 4F10, which significantly dampens its stress alleviating ability. Our genetic and integrated multi-omics studies confirm the involvement of host genetic effects in reshaping a stress-alleviating root microbiome during drought, and provide mechanistic insights into Rhizobiaceae mediated abiotic stress protection.

Plant roots are surrounded by highly diverse soil microbial communities, and their coevolution is crucial for plant fitness and the function of rhizosphere ecosystems^{1–4}. Different plant ecotypes or cultivars share common and sometimes heritable microbiome features^{5–7}, indicating that hosts can selectively shape a “core microbiome”. In addition, plants can even actively reshape their microbiome in response to various stresses to enhance fitness⁸. Currently, our understanding of the regulatory links between host genes and microbial ecosystems and their consequences for plant fitness is still in its infancy. Drought is one of the most destructive abiotic stresses and a significant threat to agricultural production

worldwide. It has been estimated that more than 50% of arable land will be affected by drought by 2050⁹. Numerous studies suggest that drought also profoundly disrupts soil microbiomes and plant-associated microbiomes across various plant species and ecosystems^{10,11}, and that prolonged drought stress even dampens root microbiome resilience after drought recovery¹². However, currently, we still lack genetic evidence to support whether plant genetic effects are positively involved in shaping drought-triggered microbiome changes. Studying how plant genetic effects positively reshape root-associated microbiomes under drought stress will further our understanding of how plant-microbiome holobionts adapt

¹Shenzhen Key Laboratory of Plant Genetic Engineering and Molecular Design, Institute of Plant and Food Science, Department of Biology, School of Life Sciences, Southern University of Science and Technology (SUSTech), Shenzhen, Guangdong, China. ²Department of Immunology and Microbiology, School of Life Sciences, Southern University of Science and Technology (SUSTech), Shenzhen, Guangdong, China. ³These authors contributed equally: Zhenghong Wang, Zewen Li. ✉ e-mail: songy3@sustech.edu.cn

to drought and help develop microbiome engineering approaches to combat drought.

Plant genetic approaches provide powerful tools for studying how plants shape the microbiome. For example, our previous genetic screening identified the receptor-like kinase FERONIA which can regulate the colonization of beneficial *Pseudomonads*¹³. A pioneering genetic study demonstrated that disruption of distinct hormone signaling pathways in *Arabidopsis* mutants could alter the microbiome structure¹⁴. This study provided the first solid genetic evidence that plants can shape their root-associated microbiome. Moreover, by using genetic mutants to suppress multiple plant immune pathways, previous studies revealed the critical roles of innate immunity in maintaining microbiome homeostasis and plant health^{15,16}. Researchers have further revealed that various plant signaling pathways influence the microbiome structure, including epigenetic modifications^{17,18}, small RNA generation¹⁹, and diverse metabolic pathways^{20,21}. Although plant genetic tools have been extensively employed to dissect the regulatory mechanisms of the microbiome composition under normal conditions, genetic studies regarding how plants positively reshape microbiomes under drought stress are still lacking.

Numerous studies indicate that the plant host might be involved in orchestrating drought-induced root microbiome changes, although we still lack genetic evidence to support this. For example, drought stress has a much stronger influence on the composition of root-associated microbiomes than it does on bulk soil microbiomes¹⁰. Furthermore, the effects of drought on root-associated microbiomes vary across different plant development stages (flowering or not)²², indicating the impact of plant developmental stages on drought-induced reshaping of the microbiome. Integrated multi-omics approaches have suggested that glycerol 3-phosphate (G3P) and iron are potential metabolic cues affecting drought-induced dynamic assembly of the root microbiome^{22,23}. Studies in different wild species and crops have demonstrated that drought stress can enrich certain microbes, such as Actinobacteria (especially *Streptomyces*), which may enhance the drought tolerance of plants^{12,22,24}. A recent study inoculated 21 different tree species with different soil microbiomes and reported that inoculation of soil microbiomes sourced from drier, warmer, or colder sites promoted plant survival in the context of subsequent drought, heat, or cold stress, respectively⁴. These studies indicate that plants might be able to “cry for help” to shape a drought-alleviating microbiome. Further genetic studies under stress conditions could provide a deeper mechanistic understanding of how the host positively regulates drought-triggered microbiome changes, which is crucial for harnessing the microbiome to combat drought stress²⁵.

Root hairs are essential for water and nutrient uptake and serve as the frontline cells of root microbiome interactions^{26,27}. In addition, plants secrete approximately 20–30% of their photosynthetic carbon source as root exudates into the rhizosphere, with root hairs playing a vital role in this process²⁸. We thus hypothesized that root hairs might orchestrate microbiome sculpting upon drought stress during long-term evolution. Moreover, the well-characterized genetic regulatory pathways of root hair development enabled us to obtain mutants with different root hair densities to study their effects on drought-induced microbiome changes. The master transcription factor GLABRA 2 maintains a non-hair cell fate and negatively regulates root hair initiation and development²⁹. In contrast, a group of upstream basic helix-loop-helix (bHLH) transcription factors, including *ROOT HAIR DEFECTIVE 6* (*RHD6*) and its homolog gene *RHD6-LIKE 1* (*RSL1*), positively regulate the expression of two closely related downstream bHLH transcription factors (*RSL2* and *RSL4*) to promote root hair development³⁰. The *rs12 rs14* double mutant shows complete loss of root hairs³¹.

In this work, we thus utilized genetic mutants with different root hair densities to dissect whether plant genetic effects regulate drought-triggered microbiome changes. The objectives of this study

were as follows: (1) to decipher the effects of root hair developmental regulators on the dynamic assembly of the microbiome in response to drought stress; (2) to identify keystone taxa or microbes influenced by root hair regulators under drought stress, and their potential relevance for plant fitness; (3) to investigate the potential metabolic and genetic mechanisms related to beneficial root microbiome interactions under stress.

Results

Mutants with altered root hair densities affect microbiome-mediated drought protection in natural soil

Autoclaving is an effective way to eradicate large parts of soil microbiomes and has been widely used to preliminarily test the involvement of the microbiome in influencing host phenotypes^{32,33}. To dissect whether root hair development-related mutants also orchestrate drought-induced microbiome changes to confer drought protection effects, we analyzed plant performance under drought stress in both sterilized and non-sterilized natural soils (Fig. 1a). To provide a relatively diverse natural soil microbiome and enrich potential drought adapted soil microbes, we mixed natural soils from a tropical rainforest soil (high microbial diversity) and a dry hot valley in southwest China (containing drought-adapted microbes) as our experimental soil (Supplementary Fig. 1). We chose to use the *gl2* (hairy mutant) and *rs12 rs14* double mutant (hairless mutant) as genetic tools to manipulate the root hair density (Fig. 1b, c). They are well-known upstream regulators specific for root hair development without side effects on lateral and primary root development (Supplementary Fig. 2). We tested the drought tolerant phenotypes of *rs12 rs14* double mutant (complete loss of root hairs), *gl2* mutant (significantly increased root hair density) and wild-type (Col-0) plants in the natural soil (non-sterilized) and autoclaved (sterilized) natural soil (Fig. 1d). To evaluate the effects of our drought treatment (withholding water) on natural soil, we measured the dynamic changes in the soil water content (gravimetric water content) at the indicated time points (Supplementary Fig. 3). The soil water content gradually decreased to approximately 25% after 12 days of withholding water for all of the genotypes, whereas it was maintained at ~75% for all of the control plants.

Notably, all of the genotypes grown in sterilized natural soil were more susceptible to drought stress than the plants in the non-sterilized soil (Fig. 1d, e). This strongly suggests that an intact soil microbial community is essential for protecting plants from drought stress, regardless of their genotype. However, the hairy mutant *gl2* presented the greatest drought tolerance (relative fresh weight in the drought-treated group compared with the control group) in non-sterilized soil at 12 days after withholding water, while it was the most drought-susceptible mutant in sterilized soil (Fig. 1d, e). This suggests that *gl2* mutant has stronger microbiome-mediated drought protection. In contrast, the hairless mutant *rs12 rs14* presented the highest drought tolerance in sterilized soil but the lowest tolerance in non-sterilized soil, suggesting that it had the weakest microbiome-mediated drought protection effect (Fig. 1d, e). To evaluate whether the root hair regulator-mediated regulation of the drought-alleviating microbiome was reproducible in other soils, independent soil experiments were performed using soil from a farm in Guangzhou (collected from approximately 1200 km away from the previous soil harvesting sites). We observed a very similar trend that the hairy mutant *gl2* had the greatest microbiome-mediated drought protection effect (Supplementary Fig. 4), which strongly suggested that the effect of *gl2* on the root microbiome is robust among different rhizosphere ecosystems. Moreover, we also tested a few more mutants that suppress root hair development (*rh17*, *cpc*^{34,35}; Supplementary Fig. 4), which also presented similar decreases in microbiome-mediated drought protection effects. Collectively, our data suggest that mutants affecting root hair development also influence the microbiome-mediated drought protection of the host.

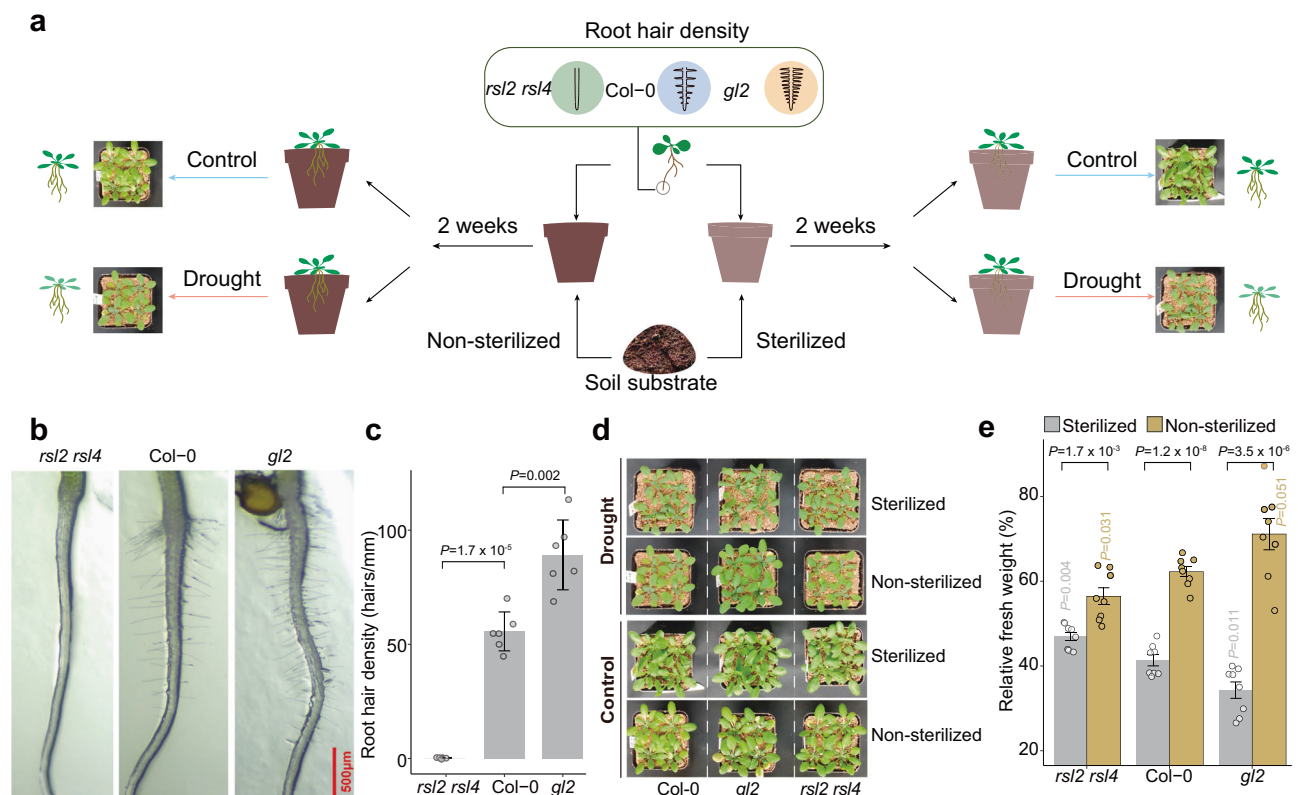


Fig. 1 | The drought-tolerant phenotypes of root hair-related mutants and wild type (Col-0) in sterilized and Non-sterilized soil. a A diagram illustrating the design of drought treatment experiments in sterilized and non-sterilized natural soil. **b** Phenotypes and **(c)** quantifications of root hair densities of the 5-day-old *rs/2 rs/4*, Col-0, and *gl/2* (two-sided Student's *t* test). Data represent mean (bar) \pm standard error of the mean (error bar). The experiment was repeated twice with consistent results ($n = 6$ biological replicates). **d** Drought tolerant phenotype at 12 days after withholding watering in Col-0 and root hair-related mutants under

sterilized and non-sterilized soil. **e** Quantification of the relative fresh weight (fresh weight of plant shoots grown in the drought-treated group relative to the average shoot fresh weight in the control group) in each genotype at 12 days after withholding watering ($n = 8$). Three independent experiments showed similar results for **(d)** and **(e)**. Results are presented as mean \pm stand error of the mean (SEM). The *P* values between each mutant and Col-0 were labeled above each bar (two-sided Student's *t* test).

Mutants affecting root hair density harbor distinct microbiomes under drought stress

To thoroughly reveal how root hair-related mutants affect drought-induced microbiome changes, we conducted 16S rRNA gene amplicon sequencing for root-associated microbiome samples from different compartments, including both root (thoroughly washed roots), rhizosphere (closely attached soil on the root surface) and bulk soil (without plant growth) under drought conditions and the control (Fig. 2). A total of 15,332,970 reads were obtained from 70 samples, including rhizosphere, root, and bulk soil samples ("Methods", Supplementary Data 1). After filtering, denoising, chimera removal, and taxonomic annotation using DADA2³⁶, we obtained 5174 amplicon sequence variants (ASVs) from all of the samples (Supplementary Data 2). We observed clear differences in microbiome composition between root-associated microbiomes and bulk soil (BS) samples at both the phylum and family levels, indicating a rhizosphere effect on microbiome composition (Supplementary Fig. 5a, b). We found that *gl/2* enhanced alpha diversity in the root microbiomes under control conditions (Fig. 2a).

Principal coordinate analysis (PCoA) based on Bray–Curtis dissimilarities was performed for all of the samples. Our results revealed that samples belonging to different compartments (bulk soil, root, and rhizosphere) were clustered into distinct groups (Fig. 2b; $R^2 = 0.31$, $P = 0.001$), and there was a significant separation among the treatments (Fig. 2b; $R^2 = 0.03$, $P = 0.005$). Both drought stress and root compartments (root and rhizosphere) had substantial effects on microbiome composition, which is consistent with previous reports^{22,37}. Interestingly, we found that plant genotype also

significantly influences the microbiome composition (Fig. 2b; $R^2 = 0.03$, $P = 0.017$). These results suggest that both mutants, in terms of root hair development (genotypes) and drought stress (treatments), jointly shape root-associated microbiome changes.

The *gl/2* mutant causes a deterministic root microbiome assembly process upon drought stress

Analyzing the assembly cues of microbial communities helps us understand whether genetic mutations in plants cause deterministic community changes³⁸. We followed the framework of quantitatively inferring Community Assembly Mechanisms by Phylogenetic-bin-based null model analysis (iCAMP) to assess microbiome assembly processes³⁹. We calculated the β -nearest taxon index (β NTI) in the microbiome of root hair-related mutants ($|\beta$ NTI| > 2 indicates a deterministic process³⁸). For the rhizosphere samples from all of the genotypes, a stochastic process ($-2 < \beta$ NTI < 0) governed the microbiome assembly under both the control and drought conditions (Fig. 2c). The Bray-Curtis-based Raup-Crick index (RC_{bray}) is used to classify the contribution of different stochastic ($-2 < \beta$ NTI < 2) community assembly cues in iCAMP⁴⁰. This approach creates a re-scaled probability metric ranging from -1 to 1 , indicating whether local communities are more dissimilar (approaching 1) or less dissimilar (approaching -1) than expected by random chance⁴¹. In rhizosphere samples, dispersal limitation (β NTI < -2 and $RC_{bray} > 0.95$) governed the stochastic process in all genotypes under drought (Fig. 2d).

In contrast, the assembly of root microbiome was almost completely governed by a deterministic process in *gl/2* (β NTI < -2) under

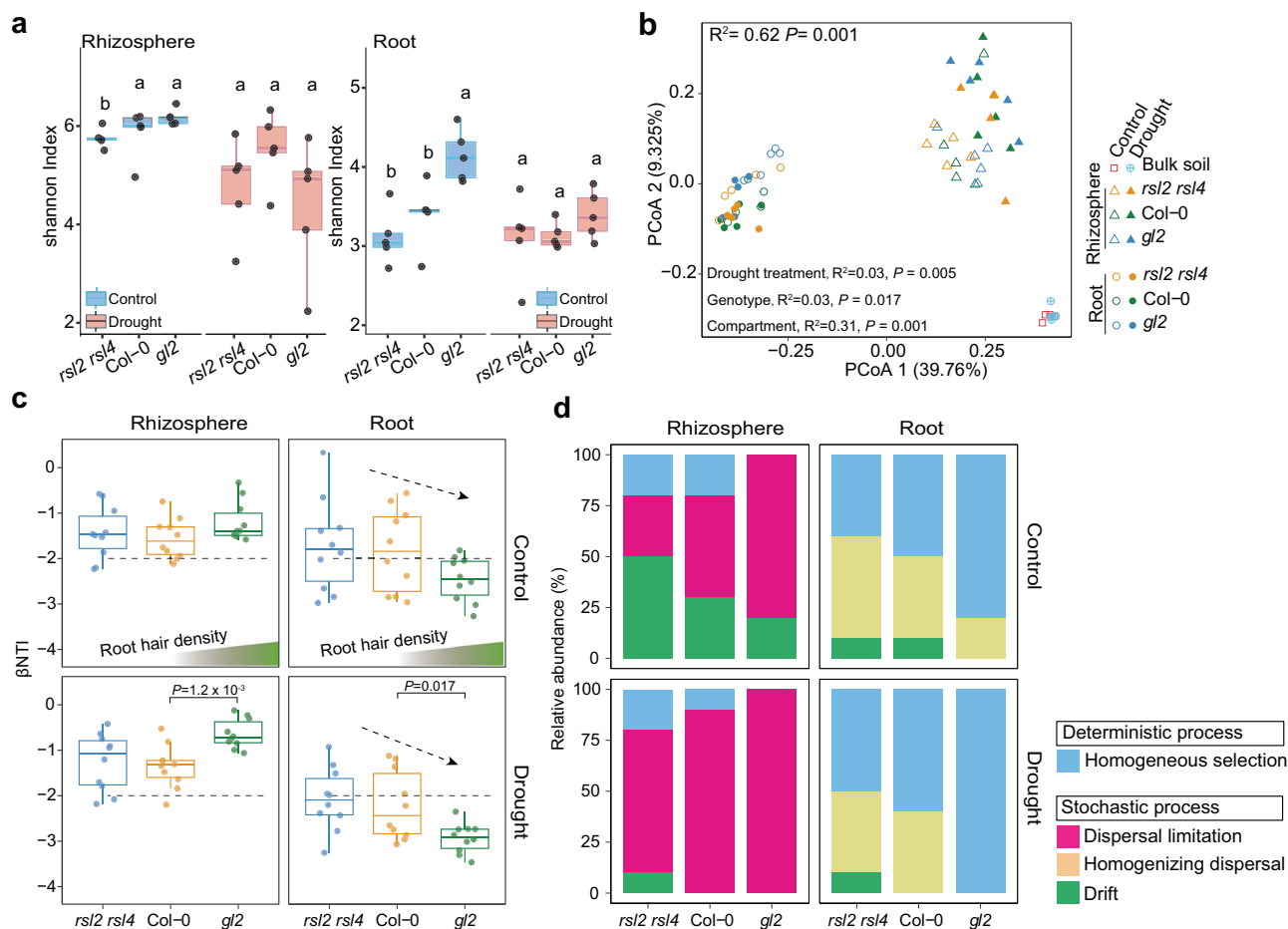


Fig. 2 | Root hair related mutants shift microbiome composition in responses to drought. **a** The Shannon index of microbial communities in root and rhizosphere samples. Different lowercase letters indicate significant differences among genotypes (one-way ANOVA followed by LSD test, P -values were corrected using Bonferroni method, $n = 5$). **b** Principal coordinates analysis (PCoA) based on Bray–Curtis dissimilarity (PERMANOVA by Adonis, $n = 5$). **c** The β -nearest taxon indexes (β NTI) in different genotypes. Each dot represents the β -nearest taxon index calculated from each pairwise sample ($n = 10$ paired comparison). The

dashed line represents the cutoff for determining deterministic ($|\beta$ NTI| > 2) and stochastic processes ($|\beta$ NTI| < 2). Box plots show the median (horizontal bar), 25th (bottoms of boxes), and 75th (tops of boxes) quartiles range (QR), as well as non-outlier data value (upper and lower whiskers). Only the significant differences (marked with P -value) of β NTI values between root hair mutants and *Col-0* are listed above the bars (two-sided Student's t test). **d** The percentage of the relative influence of each community assembly cue was defined as the proportion of pairwise samples governed by each process.

both drought and control conditions (Fig. 2c). The contribution of deterministic (mainly for homogeneous selection) process gradually increased from *rsL2* *rsL4* (hairless) and *Col-0* to *gl2* (hairy), which is correlated with an increase in root hair density (Fig. 2c). Homogeneous selection means that the overall environmental effects on community assembly are non-selective for all (or most) microbes, thus competitive exclusion within the microbial community (between different microbes) would mainly drive community assembly³⁹. This indicates that *gl2* mutant (hairy) might have overall homogeneous effects on root microbiome through root exudates or other physiological effects. Our results provide evidence that plant genetic effects in the deterministic assembly of root microbiome under drought stress.

Rhizobiaceae are biomarker taxa affected by root hair-related genetic regulators under drought

To further explore the key taxa influenced by root hair-related mutants, we analyzed the relative abundance of different taxonomic levels among the genotypes. Considering that we only observed a deterministic assembly process affected by genetic mutations in the root microbiome rather than the rhizosphere microbiome (Fig. 2c, d), we subsequently focused on the root microbiome for further analysis. Linear discriminant analysis effect size (LEfSe) is a widely used

biomarker characterization method that first uses a nonparametric test to identify differentially abundant species among groups and then estimates the effect size of each differentially abundant species on the basis of an LDA model (averaging the differences between class means with the differences between class means along the first linear discriminant axis)⁴². Notably, we identified Rhizobiaceae as the biomarker family in *gl2* (Fig. 3a), with the highest abundance among all biomarker families identified in distinguishing the three genotypes (Fig. 3b). Moreover, we found that the abundance of Rhizobiaceae was slightly but significantly higher in *gl2* than in *Col-0* and *rsL2* *rsL4* under drought stress (Supplementary Fig. 5b, c, d).

Our differential abundance (DA) analysis of ASVs between individual mutant and *Col-0* further confirmed that multiple DA ASVs in *gl2* belong to Rhizobiaceae. For example, among a total of 5 DA ASVs enriched in the roots of *gl2* under drought stress, 3 belong to Rhizobiaceae (Fig. 3c). Only 1 ASV (belonging to Comamonadaceae) was enriched in the roots of *rsL2* *rsL4* (Fig. 3d). Overall, both our biomarker prediction and differential abundance analysis support that Rhizobiaceae are major biomarker taxa affected by root hair-related mutants under drought stress. To further explore whether root hair-related mutants affect the network interactions of Rhizobiaceae in the root microbiome, we constructed the co-occurrence networks on the basis

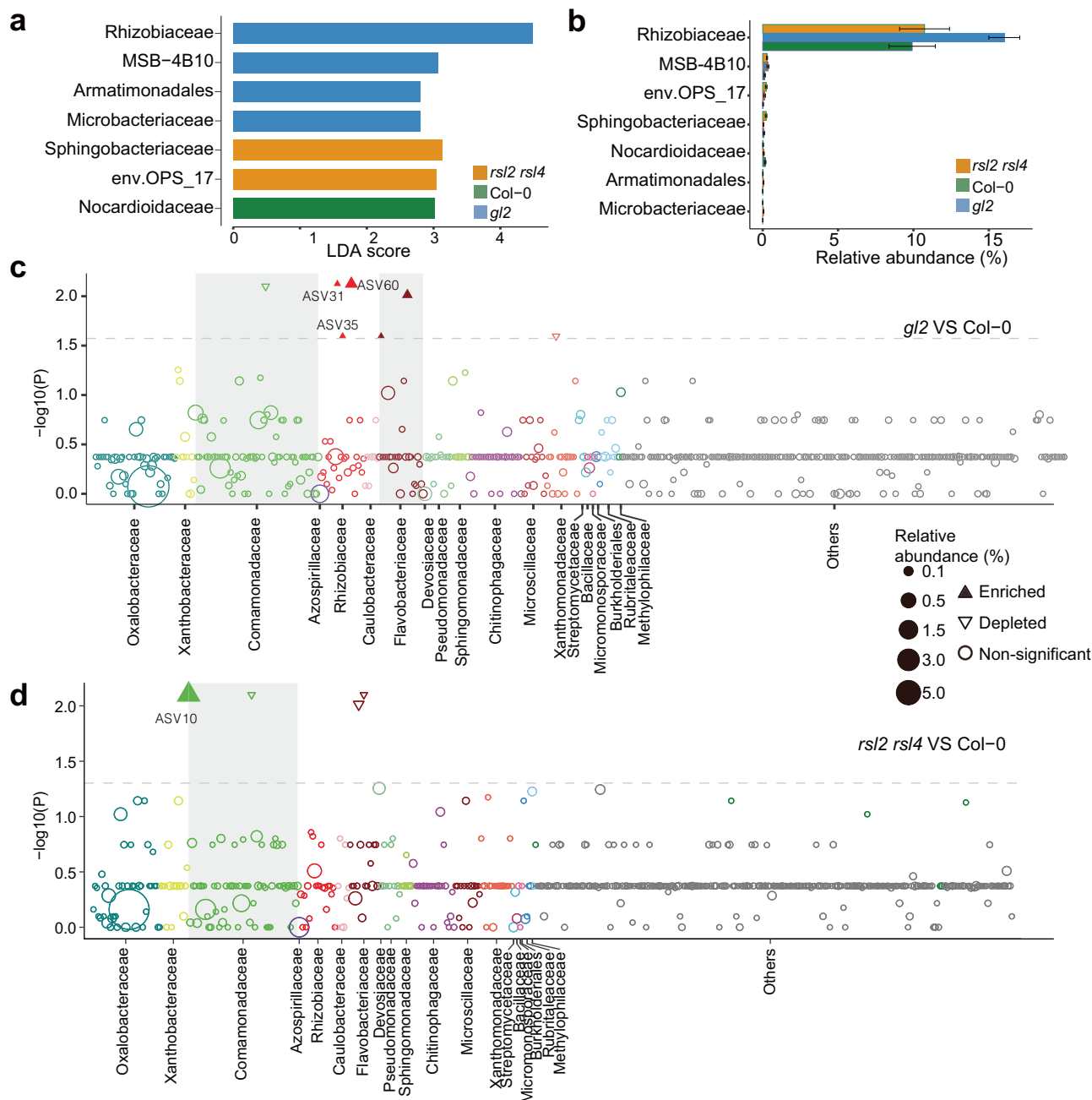


Fig. 3 | Biomarker taxa in different genotypes. a, b A total of 7 biomarker families were identified under drought conditions by Linear discriminant analysis (LEfSe) (**a**) and their corresponding relative abundances (**b**) in each genotype ($n = 5$). In the bar plot, data represent the mean (bar) \pm standard error of the mean (error bar). **c, d** Manhattan plot showing the differential abundance ASVs enriched or depleted in the roots of *g/2* (**c**) and *rsl2 rsl4* (**d**) compared to Col-0 (two-sided Wilcoxon rank

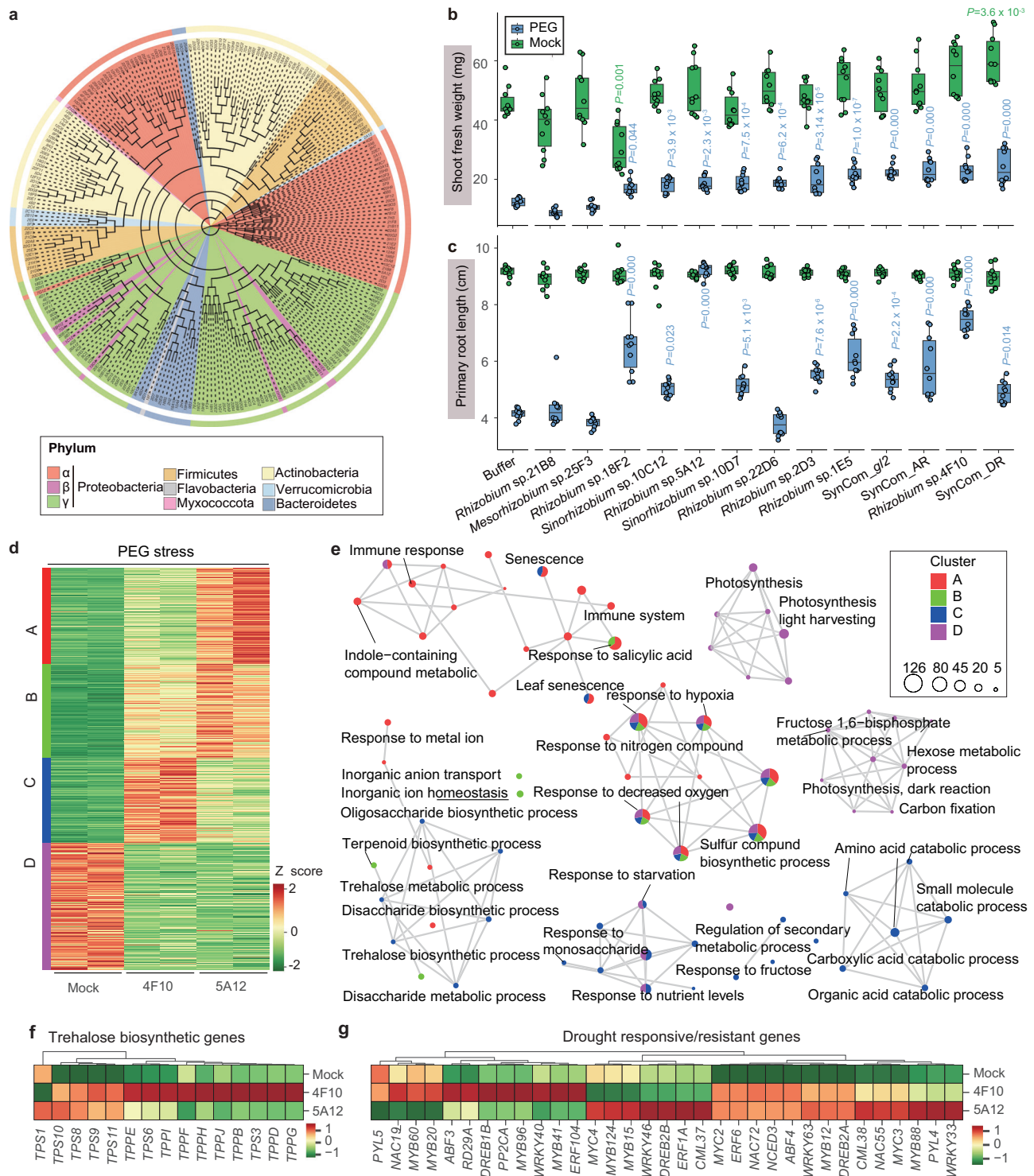
sum test, FDR adjusted $P < 0.05$) under drought conditions ($n = 5$). Each dot or triangle represents each ASV. ASVs were colored according to the taxonomic family. The size of each dot or triangle represents the relative abundance of each ASV. Solid upward triangles indicate the ASVs enriched in the roots of the mutants. Hollow downward triangles represent the ASVs depleted in the mutants.

of Spearman's correlations (with a correlation coefficient threshold of 0.7, $P_{\text{FDR}} < 0.05$) (Supplementary Fig. 6). We found that the *g/2* root microbiome has more network edges and nodes under drought, indicating a more complex microbial interaction network in the roots of *g/2* (Supplementary Fig. 6 a–f). We also detected increased centrality (assessed by degree centrality) with Rhizobiaceae nodes in the roots from *rsl2 rsl4*, Col-0 to *g/2* under drought conditions (Supplementary Fig. 6g, h and Supplementary Table 1). Moreover, we identified two network hubs in *g/2* root microbiome following a previously reported method⁴³ (Supplementary Fig. 7), and both of them belonged to Rhizobiaceae (ASV17, ASV1080). Our results suggest that root hair

development regulators also affect the abundance and network importance of the Rhizobiaceae (biomarker taxa) in drought-induced microbiome dynamic changes.

Validating the stress alleviation effects of *g/2*-affected Rhizobiaceae strains

To verify whether microbes corresponding to *g/2* regulated ASVs alleviate stress via a reductionist approach, we isolated and sequenced a total of 1479 cultivated bacteria (Methods⁴⁴). We were able to obtain 265 isolates across 7 phyla and 47 families (Fig. 4a and Supplementary Data 4). We successfully aligned diverse *Rhizobium*



strains based on the 16S rRNA gene representative sequence. Among those strains, ASV31 (matched to *Sinorhizobium* sp. 10D7, also called *Ensifer*), ASV35 (*Rhizobium* sp. 22D6), and ASV60 (*Sinorhizobium* sp. 10C12) were more enriched in the roots of *gl2* than in those of Col-0 under drought (Fig. 3c). ASV17 (*Rhizobium* sp. 2D3) was the hub node ASV within the root microbial community of *gl2* (Supplementary Fig. 7). Considering that *gl2* affects the abundance and network interactions of Rhizobiaceae ASVs under drought stress, we focused on the functions of a total of 10 strains belonging to Rhizobiaceae (including 4 strains mentioned above) from our isolated microbes (Supplementary Table 2).

The polyethylene glycol (PEG) plate-based osmotic stress treatment system is widely used to mimic drought stress and has unique advantages in maintaining a gnotobiotic system. This system can be used to precisely test the effect of specific strain(s) on plant performance in a controlled environment⁴⁵. To test whether the isolated strains influence plant stress tolerance, we tested the performance of seedlings grown on 25% PEG (induced osmotic stress) and mock (no PEG) plates (Methods; Supplementary Fig. 8 and Supplementary Table 2). For the mock group, most of them did not drastically influence seedling growth (based on the measurements of shoot fresh weight and primary root length) on the mock plates (Fig. 4b, c). However,

Fig. 4 | Isolation and validation of drought-alleviating activities of diverse Rhizobiaceae strains. **a** Phylogenetic tree of all bacterial strains isolated from *Arabidopsis* roots ($n = 265$), based on 16S rRNA gene sequences (V3–V4 region). Different background colors represent isolates belonging to each Phylum. **b** Primary root length and **(c)** Shoot fresh weight were assessed for plants (Col-0) colonized by *Rhizobium* strains under different growth conditions. SynCom_DR represents the synthetic community of three DA-ASVs (ASV31: *Sinorhizobium* sp. 10D7, ASV35: *Rhizobium* sp. 22D6, ASV60: *Sinorhizobium* sp. 10C12) enriched in the roots of *gl2*. SynCom_*gl2* represents the synthetic community of three DA ASVs and one hub ASV (ASV17). SynCom_AR includes all the members of isolated Rhizobiaceae strains. $n = 10$ biological replicates from two independent experiments. Only the significant differences (marked with P -value) between inoculated plants and uninoculated(buffer) plants are listed above each bar (one-way ANOVA followed by LSD test, P -values were corrected using Bonferroni method). Box plots show the

median (horizontal bar), 25th (bottoms of boxes), and 75th (tops of boxes) quartiles range (QR), as well as non-outlier data value (upper and lower whiskers) of each index. **d** Heatmap of the differentially expressed genes (DEGs) after inoculation with different isolates. Genes are grouped into different clusters based on k -means clustering. The heatmap is colored by normalized Z scores. **e** Gene set network/cluster analysis for DEGs in **(d)** that are enriched in subnetworks like immune response, photosynthesis, primary and secondary metabolic process, and amino acid metabolism. Each node indicates a distinct pathway, and each edge (gray line) represents the overlapping genes that exist in both two connected pathways. The size of each node indicates the number of DEGs in each distinct pathway. The pie chart indicates the proportion of DEGs belonging to the gene cluster in **(d)**. **f, g** Heatmap illustration of the DEGs involved in the **(f)** trehalose biosynthesis and **(g)** drought response.

most of them enhanced the shoot fresh weight (8 of 10) and primary root length (7 of 10) of seedlings grown on 25% PEG plates (Fig. 4b, c). These findings strongly suggest that *gl2*-enriched Rhizobiaceae strains protect seedlings from osmotic stress.

The combination of multiple strains (or a synthetic community, SynCom) can better reflect the function of a microbial community^{16,46–48} and can have more robust phenotypes for agricultural applications. We thus further explored whether we can design SynComs from *gl2* affected strains to improve plant performance in response to stress. We designed a total of 3 different SynComs: a. a mixture of all three differentially abundant (DA)-Rhizobiaceae strains enriched in the roots of *gl2* (named SynCom_DR, Fig. 4b); b. all members of SynCom_DR and ASV17 (hub ASV in the roots of *gl2*) were mixed as SynCom_*gl2*; and c. we further merged all of the Rhizobiaceae strains into SynCom_AR. Although all three SynComs (Supplementary Table 2) did not significantly affect plant growth on mock plates, all of them significantly promoted shoot fresh weight and primary root length in the seedlings growing on the PEG plates (Fig. 4b, c). Those suggested that root hairs affected Rhizobiaceae strains mainly specifically influence plant performance under stressed conditions. This might differ from previously identified *Streptomyces* strains, which generally promote growth under both normal and stressed conditions¹². Notably, seedlings inoculated with SynCom_DR presented the greatest shoot fresh weight and second highest primary root length among all treatments (Fig. 4b, c and Supplementary Fig. 5e–h). To test whether our PEG plate-based screening can identify drought-alleviating strains in soil, we inoculated plants grown in peat pellet soil with several strains with strong osmotic stress protection and three designed SynComs, respectively. We found that several strains including *Rhizobium* sp. 4F10 and *Rhizobium* sp. 5A12 can also enhance plant drought tolerance in soil (Supplementary Fig. 9).

To explore the potential molecular basis underlying Rhizobiaceae-mediated stress protection in roots, we analyzed root transcriptome responses to different stress-protecting *Rhizobium* strains. We chose *Rhizobium* sp. 4F10 and *Rhizobium* sp. 5A12 as representative stress-alleviating strains for comparative RNA-seq analysis. Both strains triggered extensive transcriptome reprogramming compared with the buffer-treated group on the PEG osmotic stress plates (Fig. 4d). However, there were clear differences between the roots responses to these two strains. For example, among a total of 2361 DEGs (differentially expressed genes) (Supplementary Data 4), *Rhizobium* sp. 4F10 specifically upregulated genes were associated with Cluster C (502 genes; Supplementary Data 5). GO enrichment analysis suggested the genes whose expression was upregulated in the *Rhizobium* sp. 4F10 were associated mainly with trehalose and other monosaccharide or disaccharide biosynthesis, amino acid catabolic process, and other small molecule catabolic processes (Fig. 4e). Similarly, *Rhizobium* sp. 4F10 significantly upregulated 14 trehalose biosynthesis genes, whereas *Rhizobium* sp. 5A12 upregulated only a small subset of these genes (Fig. 4f). The DEGs whose expression was

upregulated specifically in Cluster A were enriched in immune responses (Fig. 4d, e). This might also contribute to abiotic stress tolerance because many immune genes are also rapidly and commonly upregulated by abiotic stresses [plant general stress response (GSR)]⁴⁹. A careful examination of drought tolerance genes suggested that both *Rhizobium* sp. 4F10 and *Rhizobium* sp. 5A12 broadly promote the expression of drought tolerance genes, including master stress-responsive transcription factors such as ABFs, DREBs, MYBs, WRKYs and NACs (Fig. 4g)⁵⁰. Collectively, our physiological and molecular data confirm the positive effects of Rhizobiaceae on plant stress tolerance.

***gl2* broadly shifts the function of the root microbiome and the composition of the root metabolome**

Considering that plant hormones are broadly involved in plant responses to abiotic stresses⁵¹ and that a recent study suggested beneficial microbe-induced drought protection can be blocked by a mutant suppressing ABA signaling⁴⁵, we thoroughly analyzed whether major plant hormone perception or signal transduction-related mutants can block Rhizobiaceae-mediated drought protection (Supplementary Fig. 10). We utilized *coi1-16*⁵², *eni3 eil1*⁵³, *npr1*⁵⁴ and *ost1-3*⁵⁵ to largely suppress jasmonic acid, ethylene, salicylic acid and abscisic acid signaling, respectively. We chose *Rhizobium* sp. 4F10 for the phenotypic assay because it has the highest stress-alleviating activity on PEG plates (Supplementary Fig. 8 and Fig. 4b, c). Surprisingly, we found that none of the tested hormone-related mutants were impaired in *Rhizobium* sp. 4F10 mediated stress protection. These findings indicate that Rhizobiaceae strains might protect plants through general stress-alleviating molecules independent of the tested hormone signaling pathways.

To further investigate potential microbiome functional changes that might be related to drought protection, we conducted a meta-genomic analysis of the root-associated microbiomes of different genotypes under drought conditions. We obtained an average of 23.2 Gb of raw sequencing data per sample, resulting in a total of 14.7 million predicted genes. We annotated 13,696 KEGG Orthology (KO) terms on the basis of the eggNOG database. We then filtered for KOs that were detected in more than 3 samples. This yielded 9919 KOs, which were used for downstream analysis. Our results demonstrated that root hair-related mutations significantly altered the composition of the microbial community functional genes (Fig. 5a). Interestingly, we found that genes related to transporters, arginine and proline metabolism and transcription factors were significantly enriched in *gl2* compared with Col-0, whereas genes enriched in *rs12 rs14* were related to energy and carbohydrate metabolism (Fig. 5b, c and Supplementary Table 3, 4). Furthermore, we used LefSe analysis to identify biomarker functional categories (based on KEGG annotation) within each genotype (Fig. 5d), and arginine and proline metabolism were characterized as biomarker pathways in the root microbiome of *gl2*. These findings indicate that mutants of root hair developmental regulators affect the transportation and metabolism of the root microbiome upon drought.

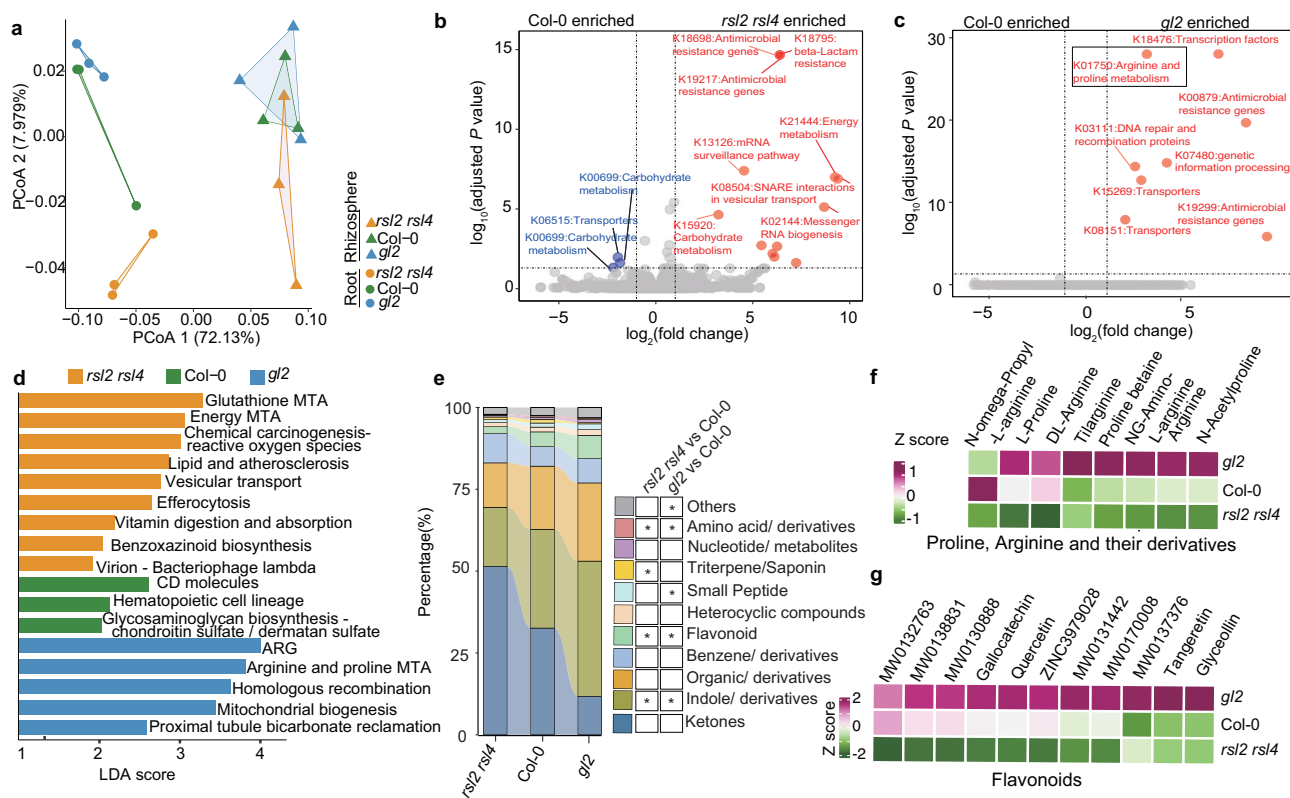


Fig. 5 | Functional profiles of root-associated microbiomes and metabolome profiling in roots. **a** Principal coordinates analysis (PCoA) of the KEGG Orthology (KO) functions based on Bray–Curtis dissimilarity [calculated using TPM (transcripts per kilobase million) counts of KOs (PERMANOVA performed by Adonis, $n = 3$)]. **b**, **c** Volcano plots visualizing the functional genes enriched or depleted (adjusted $P < 0.05$) in *rsL2 rsL4*, or *gl2* compared to *Col-0*. Red and blue dots represent the enriched genes in root hair mutants and *Col-0*, respectively. Labels of each gene were annotated based on the KEGG database. Differential analysis with a two-sided test was used for the statistical analysis. **d** Linear discriminant analysis

(LEfSe) identified biomarker function pathways within each genotype. The KEGG pathways with significant differences (LDA score > 1 and $P < 0.05$) among genotypes were listed. **e** The flow plot showed the relative abundance of metabolite classes in the root hair mutants and *Col-0*. Stars represent the specific metabolites in root hair mutants that significantly differ from *Col-0* (two-sided Student's t test). *, **, ***: represent $P < 0.05$, $P < 0.01$, $P < 0.001$, respectively. **f**, **g** Heatmap visualizing the differences in the relative abundance of individual metabolite related to (f) proline and arginine derivatives and (g) flavonoids. The heatmap is colored by normalized Z scores.

Since root hair-related mutations affect transportation and metabolism-related functions in the root microbiome, we further conducted a nontargeted metabolomics analysis to investigate the potential metabolic cues correlated with microbiome changes. A total of 3920 compounds were identified in the root samples from different genotypes (Supplementary Data 6–8). Principal component analysis (PCA) revealed significant differences in the composition of the root metabolites ($R^2 = 0.58$, $P = 0.05$, PERMANOVA by adonis) among these genotypes (Supplementary Fig. 11a). The overall abundance of amino acid, flavonoid and indole or their derivatives are gradually increased from *rsL2 rsL4* to *gl2* (Fig. 5e–g). Subsequently, differentially abundant metabolites (DMs) were identified on the basis of variable importance in projection scores ($VIP > 1.0$) and fold changes ($\log_2FC > 0$) of the relative abundances. A total of 383 DMs were identified between *gl2* and *Col-0* (Supplementary Data 9), and 990 DMs were identified between *rsL2 rsL4* and *Col-0* (Supplementary Data 10). Enrichment analysis was further conducted on the basis of the DMs in *rsL2*, *rsL4*, and *gl2*. Consistent with the increase in the relative content of overall flavonoids (Fig. 5e), the DMs in the roots of *gl2* are enriched in metabolites associated with flavonoid biosynthesis (Supplementary Fig. 11b). Flavonoids are well-known for their ability to induce the expression of rhizobia to nod genes⁵⁶, as well as the chemoattraction of rhizobia toward the roots⁵⁷. In our study, several flavonoid molecules, including tangeretin, glyceollin, quercetin and gallicolactone, are enriched in the roots of *gl2* compared with those of *Col-0* (Fig. 5g).

Genetic basis of *Rhizobium* sp. 4F10-mediated stress protection

To study the genetic mechanisms related to *Rhizobium* sp. 4F10-mediated stress protection, we successfully established a gene knockout system for the *Rhizobium* sp. 4F10 strain and sequenced the genome of this strain. Our metagenomic results indicated that arginine and proline metabolism-related functions are enriched in the root microbiome of *gl2* upon drought (Fig. 5c, d), including the proline metabolic gene K01750. This gene encodes an ornithine cyclodeaminase (OCD), which catabolizes the nonconventional proline biosynthesis pathway from L-ornithine to proline (Fig. 6a, b). We found that the *ocd* gene knockout strain of *Rhizobium* sp. 4F10 (Δocd) significantly suppressed protection effects against PEG stress, both for the primary root length and shoot fresh weight (Fig. 6c–e). To study the potential reason, we measured the growth rate of Δocd , and found that this mutation resulted in slower growth in LB medium (Fig. 6f). These findings indicate that this proline biosynthesis gene affects *Rhizobium* sp. 4F10's fitness. Considering that diverse stresses, including osmotic stress, can trigger secondary oxidative stress in both plants and bacteria⁵⁸, we further measured the tolerance of Δocd to H_2O_2 -induced oxidative stress. We found that Δocd showed significantly decreased tolerance to oxidative stress (Fig. 6g, h), which revealed a function of the OCD pathway in *Rhizobium* fitness. Our work suggests that the OCD pathway in *Rhizobium* sp. 4F10 affects bacterial fitness and stress-protecting effects on plants.

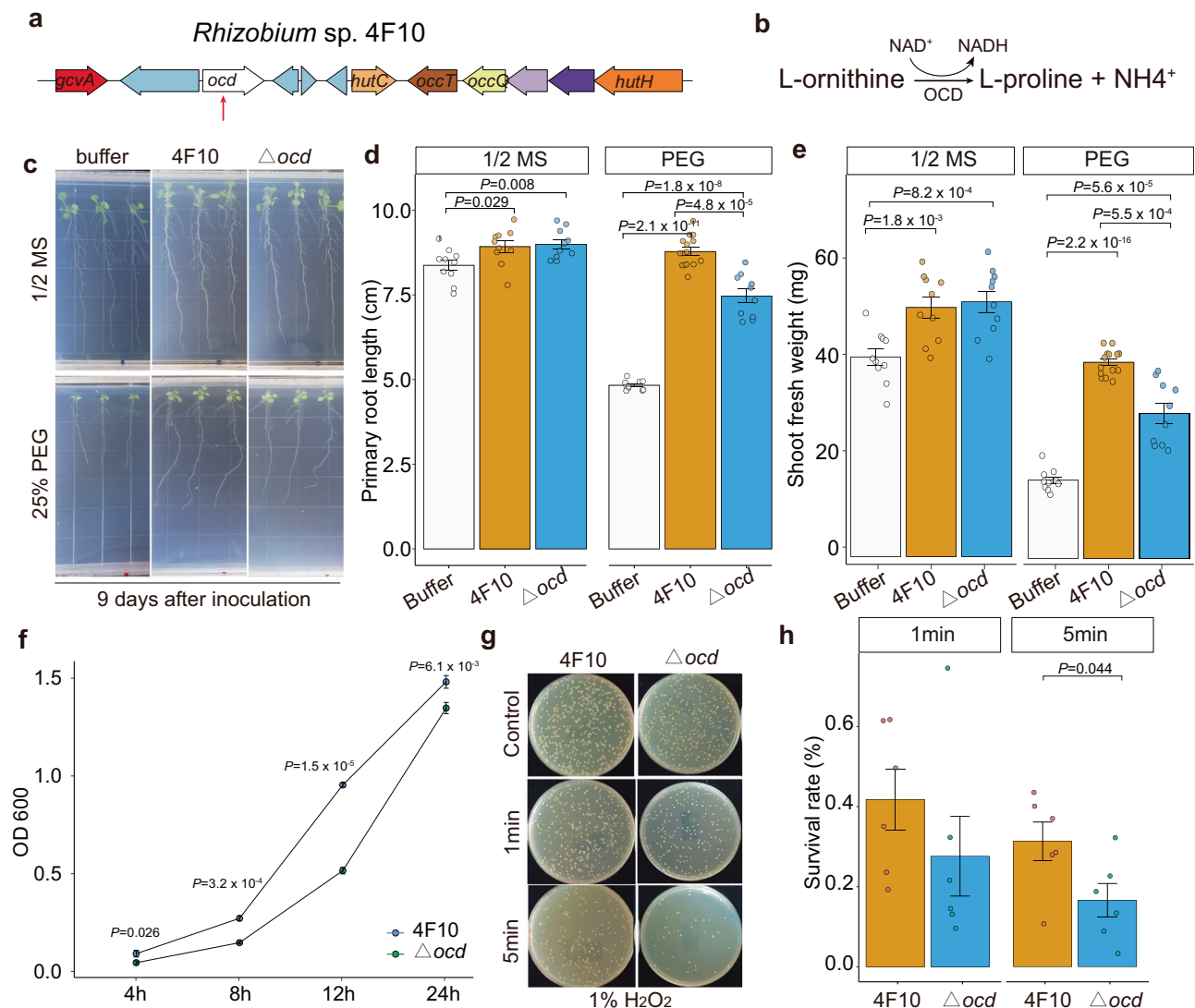


Fig. 6 | *Rhizobium* sp. 4F10 *ocd* gene is required for bacterial fitness and stress protection in plants. **a** Overview of the *ocd* gene cluster in the genome of *Rhizobium* sp. 4F10. Genes are colored based on predicted functions, and names are assigned according to the query sequence. **b** *ocd* gene mediated transformation pathway from L-Ornithine to L-Proline. **c** Phenotypes of plants (Col-0) inoculated with *Rhizobium* sp. 4F10 and Δocd grown on 1/2 MS (mock) plates or PEG plates (osmotic stress). $n = 10$ biological replicates for individual group ($n = 5$). **d** Primary root length and **(e)** shoot fresh weight were assessed for plants inoculated by *Rhizobium* sp. 4F10 or Δocd , with uninoculated plants serving as the control group ($n = 10$). Primary root length and fresh weight were rescored at 9 d and 14 d after inoculation, respectively. Data represent mean (bar) \pm standard error of the mean (error bar). Only the significant differences (marked with P -value) between different

genotypes are listed (two-sided Student's t test). Three independent experiments showed similar results. **f** Growth rate of *Rhizobium* sp. 4F10 and Δocd grown in the LB liquid medium were measured as optical density ($n = 3$). Data represent mean (dot) \pm standard error of the mean (error bar). Only the significant differences (marked with P -value) between *Rhizobium* sp. 4F10 and Δocd are shown (two-sided Student's t test). Three independent experiments showed similar results. **g** Phenotypes and **(h)** quantification results of the survival rate of *Rhizobium* sp. 4F10 and Δocd after 1 minute and 5 minutes of treatment with 1% H_2O_2 ($n = 6$). Data represent mean \pm standard error of the mean (error bar). Only the significant differences (marked with P -value) between *Rhizobium* sp. 4F10 and Δocd at different time points are shown (two-sided Student's t test).

Discussion

The root-associated microbiome substantially enhances the metabolic and genetic potential of host plants⁵⁹, which serves as the second genome of plants. Our work and those of numerous other studies confirmed that plant genetic effects contribute to the recruitment of disease-suppressive microbes^{8,13,60}. In contrast, although drought is the most serious abiotic stress that drastically disturbs the root-associated microbiome, whether and how host genetic effects reshape stress-alleviating microbes during drought are less studied. By taking advantage of elaborately designed genetic mutants with a gradient of root hair densities, we provide genetic evidence that plant root hair-related genetic regulators also orchestrate drought-triggered

microbiome changes. Considering that other root development events, such as diffusion barrier regulators, also shape microbiome composition and confer fitness benefits⁶¹, it would be interesting to further systematically test whether other mutants related to root development or architecture also impact drought-induced microbiome changes. Our work highlights the essential role of host genetic effects in reshaping a drought-alleviating microbiome and furthers our understanding of “cry for help” mechanisms during abiotic stress.

The root-associated microbiome is one of the most complex microbial communities on this planet. To comprehensively study beneficial root-microbiome interactions under stress, we need to integrate multi-omics approaches to dissect paired changes in the

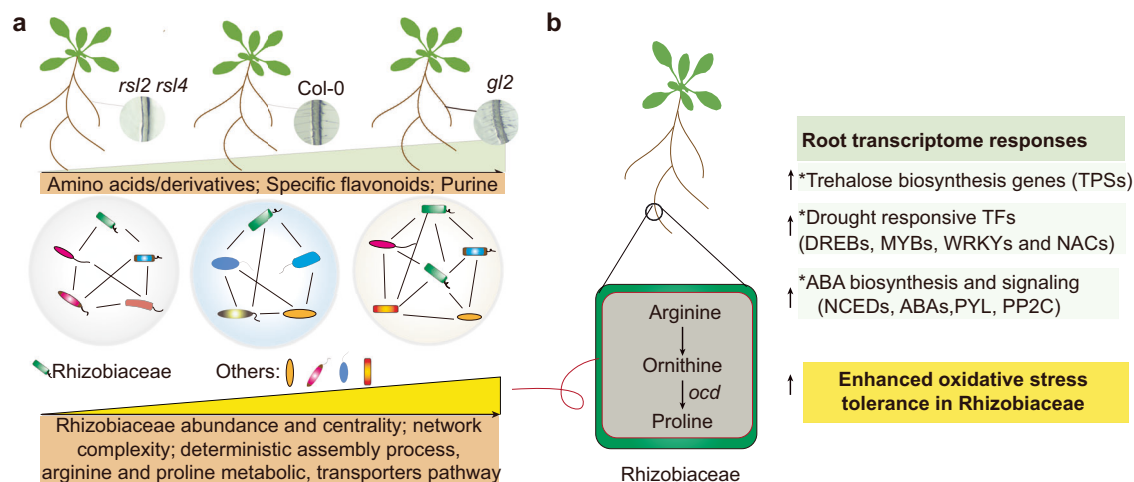


Fig. 7 | A concept model of root-*Rhizobium* interactions under drought.

a Mutants of different root hair development regulators affect root metabolites, such as amino acids and flavonoids, under drought conditions. Meanwhile, the abundance and centrality of Rhizobiaceae microbes, as well as root microbiome network complexity, also increased from *rs/2 rs/4* (hairless) to *gl/2* (hairy). The *gl/2* mutant also induced the deterministic assembly of the root microbiome and

enriched the functions of transporters and amino acid metabolism in the root microbiome. **b** *Rhizobium* sp. 4F10 broadly modulates root stress responses upon drought, priming the expression of trehalose biosynthesis and drought-responsive transcription factors (TFs). Moreover, the *ocd* gene is required for full stress protection in *Rhizobium* sp. 4F10, probably by affecting bacterial growth and oxidative stress tolerance.

host and microbiome at the same time (called holo-omics⁶²). A previous holo-omics study revealed a correlation between root-secreted G-3-P and drought-induced enrichment of monoderm bacteria²². In this study, we found that the contents of amino acids and their derivatives (especially proline- and arginine-related amino acids) are enriched in the *gl/2* (which shapes a more drought-protecting microbiome) root metabolome. These findings indicate that the increased drought tolerance of *gl/2* might be correlated with increased levels of amino acids and their derivatives (especially proline- and arginine-related amino acids) in roots, which act as osmoprotectants. Considering that amino acid metabolism has significant effects on microbiome structure and plant fitness^{63,64}, it is plausible that increased contents of amino acids and their derivatives in plant roots in response to abiotic stresses might affect root exudate composition and microbiome structure. Interestingly, we found that arginine and proline metabolism-related pathways are enriched and act as biomarkers in the *gl/2* root metagenome. This finding further indicates the correlation between elevated levels of proline- and arginine-related metabolites upon drought and enriched arginine and proline metabolic functional genes in the root metagenome. Moreover, secondary metabolites such as flavonoids and purine-related pathways are enriched in *gl/2* up-regulated metabolites (Supplementary Fig. 11). It has been well established that some flavonoids are the key determinants of the initiation of symbiosis between root hairs and Rhizobia in legumes⁶⁵. However, whether and how flavonoids affect Rhizobiaceae colonization in nonlegumes requires further genetic and metabolic investigations. With respect to the enriched purine content in *gl/2* roots, it has also been recently reported that purines contribute to shaping the stress-alleviating microbiome⁶⁶. Furthermore, transcriptome analysis revealed that *Rhizobium* sp. 4F10 broadly modulates root stress responses by priming the expression of numerous drought- or ABA-related transcription factors and trehalose biosynthesis genes (Fig. 4). Collectively, our holo-omics analyses provided integrative mechanistic insights into the extremely complex root-microbe interactions that occur in the rhizosphere ecosystem during drought (Fig. 7).

Although Rhizobiaceae is one of the most well-studied plant symbiotic bacterial families in leguminous plants, our work suggests that they confer fitness benefits and act as microbiome network hubs in the nonleguminous plant *Arabidopsis*. A previous study surveyed the

core microbiome compositions across diverse plant lineages, from non-seed to seed plants (31 plant species), and characterized *Bradyrhizobium* and *Rhizobium* as universally plant-enriched core microbiome taxa⁶⁷. Phylogenetic analysis of 1314 Rhizobiales genomes suggested that both nodulating and nonnodulating strains share common genes related to root colonization⁶⁸. The evolutionarily conserved associations between Rhizobiaceae and roots indicate their crucial roles in the structure and function of root-associated microbiomes. Moreover, a previous study in Medicago suggested that Rhizobiaceae are critical hub species in the root microbiome, and genetic mutants that lack associations with Rhizobiales present an altered microbiome structure⁴³. Interestingly, in our nonleguminous *Arabidopsis*, we also detected that root hair densities in different genotypes are correlated with relatively high colonization levels and more edges connected to Rhizobiaceae nodes, especially under drought stress. These findings further suggest the potentially conserved roles of Rhizobiaceae in mediating microbe-microbe interactions within the root microbiome network. Fortunately, we successfully established a gene knockout system in the wild-type *Rhizobium* sp. 4F10 strain, which enabled us to study the genetic determinants of stress protection in *Rhizobium*. The weakly decreased stress protection effect in the Δocd mutant is more likely due to the indirect effect of decreased fitness in this strain. Furthermore, forward genetic screening of *Rhizobium* sp. 4F10 could reveal more predominant genetic determinants of its colonization and stress protection. Our work provides an integrated research paradigm for characterizing keystone microbiome members for reductionist-based molecular mechanism studies. This emerging evidence highlights the power of microbial genetics in revealing root-microbe interaction mechanisms.

A previous study suggested that a synthetic bacterial community from a desert plant confers salt tolerance to tomato⁶⁹. These findings indicate that strains isolated from extremely abiotically stressed ecosystems could confer fitness benefits to new hosts. In this study, we successfully characterized diverse growth-promoting and stress-alleviating beneficial microbes from mixed natural soil from a tropical rainforest (which is expected to have high microbial diversity) and a dry hot valley in southwest China (which is expected to contain drought-adapted microbes). Moreover, compared with single-strain inoculation, the use of SynComs comprising multiple strains can enhance microbial drought protection effects on plants. We further

revealed that our SynComs exhibited much stronger root growth-promoting activity than most single strains did during osmotic stress. It is worth further testing the effects of our strains and SynComs on other crop species and exploring their application potential in the future. Considering that Rhizobiaceae strains have high network centrality, those strains might interact with more soil microbe nodes to form a stress-alleviating root microbiome. This finding is reminiscent of a previously reported disease-suppressive SynCom, in which each of the three individual strains did not significantly exhibit growth-promoting or disease-suppressing activity, whereas their mixed SynCom had a much stronger effect⁷⁰. Our SynCom explorations could help guide better applications of those stress-alleviating Rhizobiaceae strains.

Collectively, our work provides genetic evidence that root hair-related genetic regulators are substantially involved in reshaping drought-induced microbiome changes through the integration of plant genetics, multi-omics, reductionist-based cultureomics and monoassociation approaches (Fig. 7a). Moreover, by using natural soil from dry-hot valleys and tropical rainforests, we determined that root hairs affected Rhizobiaceae strains can help plants alleviate osmotic stress and most likely maintain the microbiome structure as keystone network nodes. This finding is consistent with the broad evolutionarily conserved associations between Rhizobiaceae and land plants⁶⁷, indicating an ancient “cry for help” strategy by terrestrial plants to engage with Rhizobiaceae. Notably, we established a genetic knockout system for *Rhizobium* sp. 4F10 and revealed the genetic mechanism related to 4F10-mediated stress protection (Fig. 7b). Our work could guide future microbiome engineering approaches to manipulate the root microbiome and combat drought stress in a changing climate.

Methods

Plant materials and growth conditions

All of the *Arabidopsis* seeds were surface sterilized for 20 min with chlorine gas (exposure to 100 mL of bleach plus 5 mL of concentrated hydrochloric acid) to eliminate potential endophytes⁷. *gl2* and *rsL2* *rsL4* were gifted from Dr. Hongwei Guo, and the *rhd7* (SALK_112105) and *cpc* (SALK_032257) mutants were obtained from ABRC. The sterilized seeds were soaked in a 0.1% agar solution and stored at 4 °C in the dark for 2 days before use. Seeds were germinated on 1/2 × Murashige and Skoog (MS) agar plates with 1% sucrose (16 h light/10 h dark, 100 μmol m⁻² s⁻¹ LED light, Fujian JIUPU BPC500H-WL plant growth chamber). Seven-day-old seedlings were subsequently transplanted into the soil. The plants were grown in a growth room under 10 h light (light intensity: 100 μmol m⁻² s⁻¹)/14 h dark conditions at 22 °C.

Natural soil collection and growth substrates

The natural soils used in this study were collected separately from the Yuanjiang Savanna Ecosystem Research Station (E102°10', N23°28') and Xishuangbanna Tropical Botanic Garden (E101°27', N21°92') of the Chinese Academy of Sciences. Visible stones, plant debris and litter were removed before the natural soil was collected. The natural soil was sieved through a 2 mm sieve. Soil from those two different locations was thoroughly homogenized and then mixed (1:1) as a natural soil mixture. Finally, we set up a mixture substrate composed of equal volumes (1:2:2:1) of mixed natural soil, commercial growth soil, vermiculite and perlite as the soil substrate for all of the natural soil experiments in this study. The soil was scooped into 6 cm by 6 cm pots in the greenhouse for plant transplantation. To sterilize the natural soil, we autoclaved the substrate twice (at 121 °C for 20 min each time) with at least a 24 h interval between two autoclaving cycles (which thoroughly killed potential germinated microbe spores after the first autoclaving). We added fertilizer once per week for the natural soil growth substrates. The natural soil from Guangdong was harvested from a farm at South China Agricultural University.

Drought treatments

The plants were subsequently transplanted from the plates into natural soil substrates on the 7th day after germination. After normal watering for three weeks, the plants within each genotype were randomly assigned to the drought or normal watering treatment (control). We conducted drought treatment by completely withholding water and randomly rotating all of the plants every day.

Sample collection

We scooped whole plants outside the pots and removed the loosely adhered soil by gently shaking the roots⁷¹. The roots from four individual plants were pooled together as a biological replicate. Roots below the shoot-root junction were immediately cut and harvested in a 50 mL Falcon tube filled with 25 mL of sterile PBS (10 mM). After shaking the Falcon tube for 20 min at 180 rpm, the roots were transferred to a new 10 mL Falcon tube filled with fresh PBS. The washing buffer was centrifuged for 20 min at 4000 × *g* (16 °C), and the resulting pellet was defined as the rhizosphere sample. For root sample collection, roots in fresh PBS were thoroughly washed and sonicated (at 40 Hz for 30 s) twice to further discard the remaining soil. The potting soil without plants and after removing 2 cm of topsoil was defined as the bulk soil. All of the samples were transferred into a new 2 mL tube, immediately frozen in liquid nitrogen, and then stored at -80 °C before DNA extraction.

DNA extraction and microbiome sequencing

DNA extraction was performed using a Power Soil DNA Isolation Kit (Qiagen, Germany) following the manufacturer's protocol. DNA samples with concentrations greater than 20 ng/μL were used for microbiome sequencing. For bacterial amplicon sequencing, the V3-V4 region of the 16S rRNA gene was amplified with the primers 349 F (5'-ACTCCTACGGGAGGCAGCA-3') and 806 R (5'-GGACTAC HVGGGTWTCTAAT-3'). Amplification was carried out under the following thermal conditions: 94 °C for 5 min, followed by 30 cycles of 94 °C for 30 s, 52 °C for 30 s, and 72 °C for 30 s, with a final extension at 72 °C for 10 min. The library was prepared following the protocol of the NEBNext® Ultra™ II DNA Library Prep Kit for Illumina® (New England Biolabs, USA). The library concentrations were determined with a Qubit 4.0 fluorometer. For amplicon sequencing, paired-end 250 bp sequencing was performed on an Illumina NovaSeq6000.

Microbiome composition-related data processing

The raw sequencing reads were filtered using fastp v.0.14.172. The adapter sequences and primers were further removed via Cutadapt v.4.0⁷³. The sequencing reads were processed using QIIME2 v.2022.2⁷⁴. Briefly, DADA2 was used to generate a table of unique amplicon sequence variants (ASVs) and their counts per sample³⁶. For taxonomic annotation, representative sequences of each ASV were assigned to the SILVA database (release 138) via a pretrained naive Bayes classifier^{75,76}. Unassigned sequences annotated as chloroplasts and mitochondria (considered as host contamination) were removed. In addition, the ASVs present in fewer than 3 samples were also removed. The retained ASVs were used for downstream analysis.

Microbial community assembly analysis

Null model analysis was carried out to evaluate the microbial community assembly process by calculating the β-nearest taxon index (βNTI)³⁸. Firstly, we calculated the observed abundance-weighted β-mean-nearest taxon distance (βMNTD_{obs}) of the pairwise community (sample) with the *comdistnt* function in the “picante” package in R⁷⁷. By randomly shuffling the tips of the phylogenetic tree, the null model expectation and distribution of βMNTD (βMNTD_{null}) were generated through 999 randomizations. The βNTI values were then calculated to quantify the standard deviations of the βMNTD_{obs} values from the distribution of βMNTD_{null} values of the pairwise community. When

$|\beta\text{NTI}| > 2$, the community assembly is interpreted as being governed by a deterministic process. Conversely, when $|\beta\text{NTI}| < 2$, community assembly is dominated by stochastic processes. Heterogeneous selection and homogeneous selection in the deterministic process were estimated with values of $\beta\text{NTI} > 2$ and $\beta\text{NTI} < -2^{40}$, respectively.

To further assess the contributions of stochastic and deterministic processes ($|\beta\text{NTI}| < 2$) to the community assembly process, a previously developed Raup-Crick index (RC_{bray}) was calculated as described previously⁷⁸. A pairwise community comparison with $|\text{RC}_{\text{bray}}| > 0.95$ indicated that dispersal led to community turnover. When $\text{RC}_{\text{bray}} > 0.95$, community turnover was dominated by dispersal limitation, whereas homogenizing dispersal occurred when $\text{RC}_{\text{bray}} < -0.95$. When pairwise community comparison with $|\beta\text{NTI}| < 2$ and $|\text{RC}_{\text{bray}}| < 0.95$, community turnover is estimated to be affected by drift alone. Collectively, the values of βNTI and RC_{bray} were integrated to assess the deterministic and stochastic processes in microbial community assembly, as well as the relative influence of each specific process.

Bacterial isolation and characterization

The roots of Col-0 plants grown in our natural soil substrates were used for isolating root-associated microbes following previously described protocols⁴⁴. The root samples were harvested from the roots at 28th days after seedling transplantation in natural soil. Roots from both the drought (14 days withholding water) and control groups were used for microbe isolation. We washed the roots three times with sterilized PBS (0.1 mol/L). After the excess liquid was absorbed from the root surface using sterilized filter paper, the roots were cut into 2 mm pieces and mixed. We placed 0.2 g of root tissue into a 1.5 mL tube with 200 μL of sterilized MgCl_2 (10 mM). The mixture was ground into a homogeneous slurry. We transferred the slurry into a sterile Falcon tube containing 25 mL of sterile MgCl_2 (10 mM) and mixed it well. After being incubated at room temperature for 10 minutes, the slurry was transferred into different bottles containing 1 L of R2A, 10% TSB (tryptic soy broth), or International Streptomyces liquid (ISP) medium for further dilution. The dilutions were selected according to the optimal range of dilutions determined by a preliminary experiment following a previous protocol⁴⁴. Then, 160 μL of diluted media was distributed into a 96-well cell plate. The plates were incubated at 28 °C for 14 days. We selected plates with visible bacterial growth in approximately 30% of the wells and transferred the bacterial culture solution in these wells to a new 96-well plate. After adding 120 μL of glycerol to the isolates, all of the plates were stored at -80°C until use.

DNA extraction of the isolates was performed using the MagaBio Plus Bacteria Genomic DNA Purification Kit (Bioer, Hangzhou, China) following the manufacturer's recommendations. PCR products targeting the V3-V4 region of the 16S rRNA gene were amplified with the primers 349 F (5'-ACTCCTACGGGAGGCAGCA-3') and 806 R (5'-GGACTACHVGGGTWTCTAAT-3'). Amplification was carried out as follows: 94 °C for 5 min, followed by 25 cycles of 94 °C for 5 seconds, 60 °C for 30 s, and 72 °C for 30 s, with a final extension at 72 °C for 10 min. The library was prepared using the NEBNext Ultra™ II DNA Library Prep Kit (New England Biolabs, USA). The library quality was determined with a Qubit 4.0 fluorometer (Thermo Scientific). Paired-end 250 bp sequencing was performed with an Illumina NovaSeq6000. We filtered out sequences with lengths of less than 380 bp. Paired-end reads of 1479 isolates were merged to obtain clean sequences. Sequence deduplication was performed using VSEARCH v2.15.2⁷⁹. The unique sequences were clustered into 265 operational taxonomic units (OTUs) at 97% similarity using UPARSE implemented with USEARCH v11.0.667⁸⁰. Representative OTU sequences were taxonomically annotated using the 16S Silva v132 database.

Metabolome profiling

For sample collection, fresh roots from 16 plants (harvested from natural soil) were pooled together as one biological replicate. A total of

three replicates from each genotype were prepared for nontargeted metabolomics analysis. The root sample collection steps were the same as those used to harvest the root samples for microbiome sequencing. After sampling, the root samples were quickly (within 5 min) and thoroughly washed in 200 mL of sterile deionized water. The resulting root tissue was immediately frozen in liquid nitrogen. The fresh weight was measured before it was stored at -80°C until further processing.

Root metabolome profiling experiment was conducted by Wuhan Metware Biotechnology Co., Ltd. (Wuhan, China), the root samples were first stored at -80°C and then thawed on ice before analysis. A 400 μL solution (methanol:water, 7:3 v/v) containing internal standard samples was added to ~20 mg of each root sample. The mixture was then vortexed for 3 min. The sample was subsequently sonicated in an ice bath for 10 min, vortexed again for 1 min, and then placed at -20°C for 30 min. Afterward, the sample was centrifuged at $13,000 \times g$ for 10 min at 4°C , and the sediment was discarded. The supernatant was then centrifuged again at $13,000 \times g$ for 3 minutes at 4°C . Finally, 200 μL of the supernatant was used for liquid chromatography-mass spectrometry (LC-MS) analysis.

The LC-MS analysis was carried out on a Shimadzu LC-30 A system (paired with TripleTOF 6600 +, SCIEX) equipped with an ACQUITY UPLC BEH C18 column (1.8 μm , 2.1 mm \times 100 mm, Waters). The analytical conditions were as follows: the mobile phases used were Milli-Q water with 0.1% formic acid (solvent A) and acetonitrile with 0.1% formic acid (solvent B), with all of the solvents being LC-MS grade. The injection volume was 2 μL . The flow rate was set at 0.4 mL/min, and the column temperature was 40°C . The capillary temperature was set at 550°C (ESI+) or 450°C (ESI-). The mass spectrometry (MS) data were acquired in the information-dependent acquisition (IDA) mode using Analyst TF 1.7.1 software (Sciex, Concord, ON, Canada). MS analysis was conducted in negative and positive ion modes with electrospray ionization. The source parameters used for MS were as follows: temperature (TEM) at 550°C ; ion source gas 1 (GAS1) at 50 psi; ion source gas 2 (GAS2) at 50 psi; curtain gas (CUR) at 35 psi; ion spray voltage floating (ISVF) at 5000 V and 4000 V for positive and negative modes, respectively; and declustering potential (DP) at 60 V or -60°V for positive and negative modes, respectively.

The original data file obtained by LC-MS was converted into mzML format via ProteoWizard software⁸¹. Peak extraction, peak alignment, and retention time correction were performed via the XCMS program⁸². The "SVR" method was used to correct the peak area. The peaks with detection rates lower than 50% in each group of samples were discarded. For metabolite annotations, the metabolic identification information was obtained by querying databases, including the database MWDB (by comparison with local standards); DB-all public databases, including Metlin (<http://metlin.scripps.edu/index.php>), HMDB, KEGG, Mona (<https://mona.fiehnlab.ucdavis.edu/>), MassBank (<http://www.massbank.jp/>); AI prediction databases (based on competitive fragmentation modeling) and metDNA. The confidence level of the identification of metabolites was determined according to the database used. For example, a confidence level of 1 means that the metabolites were identified via the database MWDB, which is based on comparison with standards. In addition, confidence levels 2 and 3 correspond to identification on the basis of the DB-all public database and AI prediction database, respectively. The identified metabolites were annotated using the KEGG Compound database (<http://www.kegg.jp/kegg/compound/>), and the annotated metabolites were then mapped to the KEGG Pathway database (<http://www.kegg.jp/kegg/pathway.html>).

For metabolome data processing, principal component analysis (PCA), which is implemented by the function `prcomp` in the "stats" package in R, was used to assess differences in root metabolites among the root hair mutants and Col-0. Differential abundance metabolites (DMs) between each mutant and Col-0 were determined by variable

importance in projection ($VIP > 1$), P -value ($P\text{-value} < 0.05$, Student's t test), and fold change ($|\log_2FC| > 0$) differences. VIP values were extracted from the orthogonal partial least squares-discriminant analysis (OPLS-DA) result, which was generated using the R package MetaboAnalystR⁸³. Before the OPLSDA analysis, the abundance data of the metabolites were log-transformed for normalization. Differentially abundant metabolites between mutants and Col-0 were annotated using the KEGG compound database (<http://www.kegg.jp/kegg/compound/>) and further mapped to the KEGG Pathway database (<http://www.kegg.jp/kegg/pathway.html>). We performed the enrichment analysis of the DEGs based on the annotation of the differential abundance metabolites to the KEGG pathways. Rich factor, which represents the ratio of differentially abundant metabolites in a specific pathway relative to the total annotated metabolites in that pathway, was used to assess the enrichment degree of each pathway. A heatmap showing the relative abundance of differentially abundant metabolites between the mutant and Col-0 strains was generated via the “ComplexHeatmap” package in R⁸⁴.

Metagenomic sequencing and data analysis

Approximately 0.2 µg of DNA per sample was used for library preparation and shotgun metagenomic sequencing. Library quality assessment was performed on an Agilent 5400 instrument (Agilent, USA). The 150 bp paired-end fragments were subsequently sequenced using DNBSEQ-T7. All raw metagenomic sequencing data (with an average of 23.2 Gb per sample) were quality-controlled by KneadData v.0.12.0 (<http://huttenhower.sph.harvard.edu/kneaddata>). Briefly, low-quality samples were trimmed via Trimmomatic v.0.39⁸⁵ with a quality threshold of 20 and a length threshold of 50 (SLIDINGWINDOW:4:20 MINLEN:50). The reads that were aligned to the *Arabidopsis* (TAIR10) and *human* genomes (downloaded with the command `kneaddata database -download human_genome`) were considered as host contaminants and removed using Bowtie2 v.2.4.5⁸⁶. Taxonomic classification of the clean reads was inferred using Kraken2 v.2.1.3⁸⁷. The microbial abundance at the taxonomic level (species, genus, or above) was re-estimated using bracken v.2.9⁸⁸. The clean data were assembled by MEGAHIT v.1.2.9⁸⁹, and contigs less than 200 bp in length were discarded. Gene prediction over contigs was performed using metaProdigal v.2.6.3⁹⁰. The nonredundant (NR) gene set was then generated using CD-HIT v.4.8.1⁹¹. Gene function annotations based on the eggNOG database v5.0.2 were performed by running eggNOG-mapper v.2.0.1⁹² with DIAMOND v.2.1.6. We conducted linear discriminant analysis effect size (LEfSe) analysis on clusters of orthologous groups of proteins (COGs) across all samples⁴². Differential analysis of the KEGG Orthology (KO) data was carried out via the DESeq2⁹³ package in R. The pathways associated with the annotated KOs in our study were organized on the basis of records from the website <https://www.kegg.jp/kegg/pathway.html>.

Screening for stress-alleviating microbes on PEG plates and peat soil

To match the differentially abundant (DA) ASVs from microbiome sequencing to our isolated strains, we compared the 16S rRNA gene sequence of the DA-ASVs to the reference database consisting of the 16S rRNA gene sequences of all of the isolated microbes via BLAST v.2.12.0⁹⁴. The FASTA files of the reference database were made by using makeblastdb v.2.12.0⁹⁴. The effects of the isolated strains on plant fitness were assessed via a polyethylene glycol (PEG) plate-based osmotic stress treatment system^{45,95}. Briefly, wild-type *Arabidopsis* seeds were first grown on 1/2 MS medium containing 1.2% agar and 1% sucrose after gas sterilization. Five day-old *Arabidopsis* seedlings were transferred onto mock plates (1/2 MS) and 25% PEG plates. For PEG plate preparation, normal agar plates were overlaid with a solution (without agar) containing 1/2 MS, MES buffer (6 mM) and 25% PEG (250 g per litre) and allowed to equilibrate for 12 h (overnight). The

overlay solution was freshly made every time just before use. After the seedlings were transplanted, we immediately inoculated a total of 2 µL of bacterial (single strain or SynCom) inoculum ($OD_{600} = 0.005$) onto the root surface, and $MgSO_4$ buffer was used as control. After 9 days of growth after inoculation, the plants growing on normal agar plates and PEG plates were photographed for root morphology analysis via ImageJ. All shoot fresh weight measurements were conducted 14 days after inoculation.

To validate the stress-alleviating microbes in soil (Supplementary Fig. 9), we first sterilized the commercial peat pellet soil. Seven day-old *Arabidopsis* seedlings were then transplanted into the peat soil. Plants were grown under a 10 h light ($100 \mu\text{mol m}^{-2} \text{s}^{-1}$)/14 h dark cycle at 22 °C. 16 days post-transplantation, a total of 5 mL of bacterial inoculum ($OD_{600} = 0.5$, either single strain or SynCom) was inoculated into the root zone. Withholding water for four days prior to inoculation to prevent water oversaturation. As in the PEG treatment system, $MgSO_4$ buffer was used as a control. The drought tolerance of each inoculation treatment was assessed using a drought tolerance index based on the wilt degree (5: no wilting; 4: < 25% wilted leaves; 3: 25–50% wilted leaves; 2: 50–75% wilted leaves; 1: 75–90% mostly wilted) to reflect the damage of drought stress on each plant.

RNA-seq sample preparation and data processing

The total RNA of *Arabidopsis* roots was extracted using TRIzol (Bio-Rad, USA) reagent. The high-quality mRNA was purified from total RNA using poly-T oligo-attached magnetic beads (Invitrogen, USA) and then fragmented. The resulting fragmented mRNA was used for first-strand cDNA synthesis using random hexamer primers, followed by second-strand cDNA synthesis. The library was prepared after end repair, A-tailing, adapter ligation, size selection, amplification, and purification steps. The libraries were then sequenced (PE-150 bp) on the Illumina platform. Fastp (v.0.14.1) was used to evaluate the quality of the raw reads, including the removal of reads with adapter contamination, uncertain bases, and low-quality bases⁷². The quantification of expression levels for each transcript was performed using Salmon v.1.9.0⁹⁶ against the TAIR10 *Arabidopsis* reference genome, and transcripts per million (TPM) were obtained. DESeq2 was used to identify the differentially expressed (FDR adjusted $P < 0.05$) genes (DEGs) between the control and each inoculation treatment⁹³. GO and KEGG enrichment analysis were performed using the clusterProfiler package in R⁹⁷.

Gene deletions in *Rhizobium* sp. 4F10

Genetic deletion in *Rhizobium* sp. 4F10 was created using a double-recombination method for Gram-negative bacteria. Two sets of primers were used to amplify the upstream and downstream 1000 bp flanking region of *ocd* as follows: upstream forward, 5' GATTACGAATTCGAGCTCGGaactcggttgccggtatgg 3' and upstream reverse, 5' TCAGGCTGCCCTGAGCAGcggtgcccgcattgtcat 3'; downstream forward, 5' ATGCCCGCACCGctgctcagggcagcctga 3' and downstream reverse, 5' GTCACGACGTTGTAAACGAcgcaacaagatcctcgctttg 3' (overlapping bases in capital case). Overlap PCR was performed with the upstream and downstream PCR products. The product was ligated to the Pk18mobsacB suicide vector and then transformed into *E. coli* strain DH5α. The positive colonies were selected on LB plates with gentamicin 50 µg/mL and then confirmed by colony PCR. The deletion constructs were further confirmed by Sanger sequencing. The confirmed deletion constructs were then transformed into competent *E. coli* strain WM6026, which is an auxotrophic *E. coli* strain whose growth relies on exogenously supplemented DAP, and was selected on LB plates containing gentamicin 50 µg/mL and DAP 100 µg/mL. Conjugation of the WM6026 containing the deletion constructs and *Rhizobium* sp. 4F10 was performed, then the transconjugants were selected on plates with gentamicin 50 µg/mL without DAP. Positive colonies were re-streaked, and cultured overnight in liquid plain LB. The bacterial suspension was diluted to 100× with 20% LB (containing 10%

sucrose) and cultured overnight at room temperature. The bacterial suspension was spread on LB plates containing 6% sucrose to select for the second recombination.

Statistical analysis and data visualization

All of the statistics analyses in the present study were conducted in the R v.4.1.3 environment (<http://www.r-project.org/>). For differential analysis, normality tests were performed using the Shapiro–Wilk test. Then Bartlett’s test was used to test for homogeneity of variance via the “stats” package in R. The “vegan” package in R was used to assess the alpha and beta diversity of the root-associated microbial community⁹⁸. Specifically, species richness and Shannon diversity were calculated using the *diversity* function. The differences between the root hair mutants and Col-0 were assessed via one-way ANOVA, followed by an LSD test for multiple comparisons. This analysis was performed using the *LSD.test* function in the “agricolae” package in R⁹⁹. Bray–Curtis distance matrices of microbial communities were calculated using the *Vegdist* function, and principal coordinate analysis (PCoA) plots were generated accordingly. Permutational multivariate analysis of variance (PERMANOVA) was performed with the “*adonis*” function to further assess the effects of genotype (Col-0, *gl2* and *rs12 rs14*), water regime (drought treatment and control), and compartment (bulk soil, root, and rhizosphere) on variations in microbiome composition⁹⁸. The “microeco” package in R was used to perform differential abundance tests and identify potential marker families among the three genotypes¹⁰⁰. The Wilcoxon rank sum test was used to detect the differential (FDR adjusted $P < 0.05$) ASVs (based on relative abundance) between the root hair mutants and Col-0.

For network analysis, the ASVs with a relative abundance greater than 0.01% and present in at least two samples were used for co-occurrence network construction. Spearman correlation (correlation coefficient > 0.7 , $P_{\text{FDR}} < 0.05$) analysis was conducted between paired ASVs using the “ggClusterNet” package in R¹⁰¹. Network topological parameters, including node and edge counts, positive and negative correlations, and node properties, such as degree centrality, closeness centrality, were calculated using the “igraph” package in R¹⁰². Hub nodes were identified on the basis of all three measurements of centrality using a log-normal distribution fit¹⁰³. With the exception of the network visualization, which was conducted in Gephi 0.10¹⁰⁴. The locations of the natural soil sample sites, including longitude and latitude, were visualized using ArcGIS v.10.5 (Esri, Redlands, California, USA). The elevation of Yunnan province (China) was extracted based on the WorldClim dataset¹⁰⁵. All of the other plots in the present study were generated via the “ggplot2” package in R if no specific specification¹⁰⁶. The final figures (including Supplementary Figures) were prepared in Adobe Illustrator 2020 for combining, positioning, and resizing.

Reporting summary

Further information on research design is available in the Nature Portfolio Reporting Summary linked to this article.

Data availability

All sequencing data generated in this study have been deposited in the China National Center for Bioinformation [<https://www.cncb.ac.cn>]. Raw 16S amplicon and shotgun metagenomic sequencing data were deposited under accession codes CRA014605 (PRJCA023009; <https://ngdc.cncb.ac.cn/bioproject/browse/PRJCA023009>). RNA sequencing data were deposited under CRA018179 (PRJCA027686; <https://ngdc.cncb.ac.cn/bioproject/browse/PRJCA027686>). The genome of *Rhizobium* sp. 4F10 was deposited under accession number PRJCA028834. The Non-targeted metabolomics data used in this study are available in the Metabolights database under accession code MTBLS11360. Source data underlying each figure are uploaded to <https://github.com/>

Zhenghong-Wang/Root-hair-mutants-microbiome [<https://doi.org/10.5281/zenodo.13968521>].

Code availability

Codes for this project can be found at <https://github.com/Zhenghong-Wang/Root-hair-mutants-microbiome> [<https://doi.org/10.5281/zenodo.13968521>].

References

- Wipfel, K. et al. Host preference and invasiveness of commensal bacteria in the Lotus and Arabidopsis root microbiota. *Nat. Microbiol.* **6**, 1150–1162 (2021).
- Steinauer, K. et al. Plant diversity effects on soil microbial functions and enzymes are stronger than warming in a grassland experiment. *Ecology* **96**, 99–112 (2015).
- Wang, Z. et al. Land use intensification in a dry-hot valley reduced the constraints of water content on soil microbial diversity and multifunctionality but increased CO₂ production. *Sci. Total Environ.* **852**, 158397 (2022).
- Allsup, C. M., George, I. & Lankau, R. A. Shifting microbial communities can enhance tree tolerance to changing climates. *Science* **380**, 835–840 (2023).
- Walters, W. A. et al. Large-scale replicated field study of maize rhizosphere identifies heritable microbes. *Proc. Natl. Acad. Sci. USA* **115**, 7368–7373 (2018).
- Lundberg, D. S. et al. Defining the core Arabidopsis thaliana root microbiome. *Nature* **488**, 86–90 (2012).
- Haney, C. H., Samuel, B. S., Bush, J. & Ausubel, F. M. Associations with rhizosphere bacteria can confer an adaptive advantage to plants. *Nat. Plants* **1**, 15051 (2015).
- Wang, Z. & Song, Y. Toward understanding the genetic bases underlying plants mediated “cry for help” to the microbiota. *iMeta* **1**, e8 (2022).
- Zhang, H., Sun, X. & Dai, M. Improving crop drought resistance with plant growth regulators and rhizobacteria: Mechanisms, applications, and perspectives. *Plant Commun.* **3**, 100228 (2022).
- Naylor, D., DeGraaf, S., Purdom, E. & Coleman-Derr, D. Drought and host selection influence bacterial community dynamics in the grass root microbiome. *ISME J.* **11**, 2691–2704 (2017).
- Santos-Medellin C., Edwards J., Liechty Z., Nguyen B., Sundaresan V. Drought stress results in a compartment-specific restructuring of the rice root-associated microbiomes. *mBio* **8**, (2017).
- Santos-Medellin, C. et al. Prolonged drought imparts lasting compositional changes to the rice root microbiome. *Nat. Plants* **7**, 1065–1077 (2021).
- Song, Y. et al. FERONIA restricts Pseudomonas in the rhizosphere microbiome via regulation of reactive oxygen species. *Nat. Plants* **7**, 644–654 (2021).
- Lebeis, S. L. et al. Salicylic acid modulates colonization of the root microbiome by specific bacterial taxa. *Science* **349**, 860–864 (2015).
- Pfeilmeier, S. et al. The plant NADPH oxidase RBOHD is required for microbiota homeostasis in leaves. *Nat. Microbiol.* **6**, 852–864 (2021).
- Chen, T. et al. A plant genetic network for preventing dysbiosis in the phyllosphere. *Nature* **580**, 653–657 (2020).
- Vilchez, J. I. et al. DNA demethylases are required for myo-inositol-mediated mutualism between plants and beneficial rhizobacteria. *Nat. Plants* **6**, 983–995 (2020).
- Lv, S. et al. Dysfunction of histone demethylase IBM1 in Arabidopsis causes autoimmunity and reshapes the root microbiome. *ISME J.* **16**, 2513–2524 (2022).
- Kaushal, R. et al. Dicer-like proteins influence Arabidopsis root microbiota independent of RNA-directed DNA methylation. *Microbiome* **9**, 57 (2021).

20. Huang, A. C. et al. A specialized metabolic network selectively modulates Arabidopsis root microbiota. *Science* **364**, (2019).
21. Stringlis, I. A. et al. MYB72-dependent coumarin exudation shapes root microbiome assembly to promote plant health. *Proc. Natl. Acad. Sci. USA* **115**, E5213–E5222 (2018).
22. Xu, L. et al. Drought delays development of the sorghum root microbiome and enriches for monoderm bacteria. *Proc. Natl. Acad. Sci. USA* **115**, E4284–E4293 (2018).
23. Xu, L. et al. Genome-resolved metagenomics reveals role of iron metabolism in drought-induced rhizosphere microbiome dynamics. *Nat. Commun.* **12**, 3209 (2021).
24. Fitzpatrick, C. R. et al. Assembly and ecological function of the root microbiome across angiosperm plant species. *Proc. Natl. Acad. Sci. USA* **115**, E1157–E1165 (2018).
25. de Vries, F. T., Griffiths, R. I., Knight, C. G., Nicolitch, O. & Williams, A. Harnessing rhizosphere microbiomes for drought-resilient crop production. *Science* **368**, 270–274 (2020).
26. Ruiz, S. et al. Significance of root hairs at the field scale - modelling root water and phosphorus uptake under different field conditions. *Plant Soil* **447**, 281–304 (2020).
27. Zhang, X. et al. The spatial distribution of rhizosphere microbial activities under drought: water availability is more important than root-hair controlled exudation. *New Phytol.* **237**, 780–792 (2022).
28. Holz, M., Zarebanadkouki, M., Kuzyakov, Y., Pausch, J. & Carminati, A. Root hairs increase rhizosphere extension and carbon input to soil. *Ann. Bot.* **121**, 61–69 (2018).
29. Lin, Q. et al. GLABRA2 Directly suppresses basic helix-loop-helix transcription factor genes with diverse functions in root hair development. *Plant Cell* **27**, 2894–2906 (2015).
30. Pires, N. D. et al. Recruitment and remodeling of an ancient gene regulatory network during land plant evolution. *Proc. Natl. Acad. Sci. USA* **110**, 9571–9576 (2013).
31. Yi, K., Menand, B., Bell, E. & Dolan, L. A basic helix-loop-helix transcription factor controls cell growth and size in root hairs. *Nat. Genet.* **42**, 264–267 (2010).
32. Zhou, X. et al. Interspecific plant interaction via root exudates structures the disease suppressiveness of rhizosphere microbiomes. *Mol. Plant* **16**, 849–864 (2023).
33. Yang, K. et al. RIN enhances plant disease resistance via root exudate-mediated assembly of disease-suppressive rhizosphere microbiota. *Mol. Plant* **16**, 1379–1395 (2023).
34. Hu, H. et al. AtCSLD3 and GhCSLD3 mediate root growth and cell elongation downstream of the ethylene response pathway in Arabidopsis. *J. Exp. Bot.* **69**, 1065–1080 (2018).
35. Wada, T. et al. Role of a positive regulator of root hair development, CAPRICE, in Arabidopsis root epidermal cell differentiation. *Development* **129**, 5409–5419 (2002).
36. Callahan, B. J. et al. DADA2: High-resolution sample inference from Illumina amplicon data. *Nat. Methods* **13**, 581–583 (2016).
37. Gao, C. et al. Co-occurrence networks reveal more complexity than community composition in resistance and resilience of microbial communities. *Nat. Commun.* **13**, 3867 (2022).
38. Stegen, J. C., Lin, X., Konopka, A. E. & Fredrickson, J. K. Stochastic and deterministic assembly processes in subsurface microbial communities. *ISME J.* **6**, 1653–1664 (2012).
39. Ning, D. et al. A quantitative framework reveals ecological drivers of grassland microbial community assembly in response to warming. *Nat. Commun.* **11**, 4717 (2020).
40. Zhou, J. & Ning, D. Stochastic community assembly: Does it matter in microbial ecology? *Microbiol. Mol. Biol. Rev.* **81**, 00002–00017 (2017).
41. Chase, J. M., Kraft, N. J., Smith, K. G., Vellend, M. & Inouye, B. D. Using null models to disentangle variation in community dissimilarity from variation in α -diversity. *Ecosphere* **2**, 1–11 (2011).
42. Segata, N. et al. Metagenomic biomarker discovery and explanation. *Genome Biol.* **12**, 1–18 (2011).
43. Wang, X. et al. Mycorrhizal symbiosis modulates the rhizosphere microbiota to promote rhizobia-legume symbiosis. *Mol. Plant* **14**, 503–516 (2021).
44. Zhang, J. et al. High-throughput cultivation and identification of bacteria from the plant root microbiota. *Nat. Protoc.* **16**, 988–1012 (2021).
45. Alwutayd, K. M. et al. Microbe-induced drought tolerance by ABA-mediated root architecture and epigenetic reprogramming. *EMBO Rep.* **24**, e56754 (2023).
46. Zhang, J. et al. NRT1.1B is associated with root microbiota composition and nitrogen use in field-grown rice. *Nat. Biotechnol.* **37**, 676–684 (2019).
47. Grosskopf, T. & Soyer, O. S. Synthetic microbial communities. *Curr. Opin. Microbiol.* **18**, 72–77 (2014).
48. Zhou, X. et al. Cross-kingdom synthetic microbiota supports tomato suppression of Fusarium wilt disease. *Nat. Commun.* **13**, 7890 (2022).
49. Bjornson, M., Pimprikar, P., Nurnberger, T. & Zipfel, C. The transcriptional landscape of Arabidopsis thaliana pattern-triggered immunity. *Nat. Plants* **7**, 579–586 (2021).
50. Singh, D. & Laxmi, A. Transcriptional regulation of drought response: a tortuous network of transcriptional factors. *Front. Plant Sci.* **6**, 895 (2015).
51. Suzuki, N. Hormone signaling pathways under stress combinations. *Plant Signal. Behav.* **11**, e1247139 (2016).
52. Ellis, C. & Turner, J. G. A conditionally fertile coi1 allele indicates cross-talk between plant hormone signalling pathways in Arabidopsis thaliana seeds and young seedlings. *Planta* **215**, 549–556 (2002).
53. Dolgikh, V. A., Pukhovaya, E. M. & Zemlyanskaya, E. V. Shaping ethylene response: The role of EIN3/EIL1 transcription factors. *Front. Plant Sci.* **10**, 1030 (2019).
54. Cao, H., Glazebrook, J., Clarke, J. D., Volko, S. & Dong, X. The Arabidopsis NPR1 gene that controls systemic acquired resistance encodes a novel protein containing ankyrin repeats. *Cell* **88**, 57–63 (1997).
55. Sun, Z. et al. RAF22, ABI1 and OST1 form a dynamic interactive network that optimizes plant growth and responses to drought stress in Arabidopsis. *Mol. Plant* **15**, 1192–1210 (2022).
56. Wang, L. et al. Multifaceted roles of flavonoids mediating plant-microbe interactions. *Microbiome* **10**, 233 (2022).
57. Hassan, S. & Mathesius, U. The role of flavonoids in root-rhizosphere signalling: opportunities and challenges for improving plant-microbe interactions. *J. Exp. Bot.* **63**, 3429–3444 (2012).
58. Shabala, S. & Shabala, L. Ion transport and osmotic adjustment in plants and bacteria. *Biomol. Concepts* **2**, 407–419 (2011).
59. Wang, N. R. & Haney, C. H. Harnessing the genetic potential of the plant microbiome. *Biochemist* **42**, 20–25 (2020).
60. Bakker, P. A., Pieterse, C. M., de Jonge, R. & Berendsen, R. L. The soil-borne legacy. *Cell* **172**, 1178–1180 (2018).
61. Salas-González, I. et al. Coordination between microbiota and root endodermis supports plant mineral nutrient homeostasis. *Science* **371**, eabd0695 (2021).
62. Xu, L. et al. Holo-omics for deciphering plant-microbiome interactions. *Microbiome* **9**, 1–11 (2021).
63. Liu, X. et al. Phyllosphere microbiome induces host metabolic defence against rice false-smut disease. *Nat. Microbiol.* **8**, 1419–1433 (2023).
64. Liu, Y. et al. Amino acid availability determines plant immune homeostasis in the rhizosphere microbiome. *mBio* **14**, e03424–03422 (2023).
65. Bag, S., Mondal, A., Majumder, A., Mondal, S. K. & Banik, A. Flavonoid mediated selective cross-talk between plants and beneficial soil microbiome. *Phytochem. Rev.* **21**, 1739–1760 (2022).

66. Zheng, Y. et al. Purines enrich root-associated *Pseudomonas* and improve wild soybean growth under salt stress. *Nat. Commun.* **15**, 3520 (2024).
67. Yeoh, Y. K. et al. Evolutionary conservation of a core root microbiome across plant phyla along a tropical soil chronosequence. *Nat. Commun.* **8**, 215 (2017).
68. Garrido-Oter, R. et al. Modular Traits of the Rhizobiales Root Microbiota and Their Evolutionary Relationship with Symbiotic Rhizobia. *Cell Host Microbe* **24**, 155–167 (2018).
69. Schmitz, L. et al. Synthetic bacterial community derived from a desert rhizosphere confers salt stress resilience to tomato in the presence of a soil microbiome. *ISME J.* **16**, 1907–1920 (2022).
70. Berendsen, R. L. et al. Disease-induced assemblage of a plant-beneficial bacterial consortium. *ISME J.* **12**, 1496–1507 (2018).
71. Bulgarelli, D. et al. Revealing structure and assembly cues for *Arabidopsis* root-inhabiting bacterial microbiota. *Nature* **488**, 91–95 (2012).
72. Chen, S., Zhou, Y., Chen, Y. & Gu, J. fastp: an ultra-fast all-in-one FASTQ preprocessor. *Bioinformatics* **34**, i884–i890 (2018).
73. Martin, M. Cutadapt removes adapter sequences from high-throughput sequencing reads. *EMBnet J.* **17**, 10–12 (2011).
74. Bolyen, E. et al. Reproducible, interactive, scalable and extensible microbiome data science using QIIME 2. *Nat. Biotechnol.* **37**, 852–857 (2019).
75. Quast, C. et al. The SILVA ribosomal RNA gene database project: improved data processing and web-based tools. *Nucleic Acids Res.* **41**, D590–D596 (2013).
76. Wang, Q., Garrity, G. M., Tiedje, J. M. & Cole, J. R. Naive Bayesian classifier for rapid assignment of rRNA sequences into the new bacterial taxonomy. *Appl. Environ. Microbiol.* **73**, 5261–5267 (2007).
77. Kembel, S. W. et al. Picante: R tools for integrating phylogenies and ecology. *Bioinformatics* **26**, 1463–1464 (2010).
78. Stegen, J. C. et al. Quantifying community assembly processes and identifying features that impose them. *ISME J.* **7**, 2069–2079 (2013).
79. Rognes, T., Flouri, T., Nichols, B., Quince, C. & Mahe, F. VSEARCH: a versatile open source tool for metagenomics. *PeerJ* **4**, e2584 (2016).
80. Edgar, R. C. UPARSE: highly accurate OTU sequences from microbial amplicon reads. *Nat. Methods* **10**, 996–998 (2013).
81. French, W. R. et al. Wavelet-based peak detection and a new charge inference procedure for MS/MS implemented in ProteoWizard's msConvert. *J. Proteome Res.* **14**, 1299–1307 (2015).
82. Benton, H. P., Want, E. J. & Ebbels, T. M. Correction of mass calibration gaps in liquid chromatography-mass spectrometry metabolomics data. *Bioinformatics* **26**, 2488–2489 (2010).
83. Chong, J. & Xia, J. MetaboAnalystR: an R package for flexible and reproducible analysis of metabolomics data. *Bioinformatics* **34**, 4313–4314 (2018).
84. Gu, Z. Complex heatmap visualization. *iMeta* **1**, (2022).
85. Bolger, A. M., Lohse, M. & Usadel, B. Trimmomatic: a flexible trimmer for Illumina sequence data. *Bioinformatics* **30**, 2114–2120 (2014).
86. Langmead, B. & Salzberg, S. L. Fast gapped-read alignment with Bowtie 2. *Nat. Methods* **9**, 357–359 (2012).
87. Wood, D. E., Lu, J. & Langmead, B. Improved metagenomic analysis with Kraken 2. *Genome Biol.* **20**, 257 (2019).
88. Lu, J., Breitwieser, F. P., Thielen, P. & Salzberg, S. L. Bracken: estimating species abundance in metagenomics data. *PeerJ Comput. Sci.* **3**, (2017).
89. Li, D., Liu, C. M., Luo, R., Kunihiro, S. & Tak-Wah, L. MEGAHIT: an ultra-fast single-node solution for large and complex metagenomics assembly via succinct de Bruijn graph. *Bioinformatics* **31**, 1674–1676 (2015).
90. Hyatt, D., LoCascio, P. F., Hauser, L. J. & Uberbacher, E. C. Gene and translation initiation site prediction in metagenomic sequences. *Bioinformatics* **28**, 2223–2230 (2012).
91. Li, W. & Godzik, A. Cd-hit: a fast program for clustering and comparing large sets of protein or nucleotide sequences. *Bioinformatics* **22**, 1658–1659 (2006).
92. Huerta-Cepas, J. et al. eggNOG 5.0: a hierarchical, functionally and phylogenetically annotated orthology resource based on 5090 organisms and 2502 viruses. *Nucleic Acids Res.* **47**, D309–D314 (2019).
93. Love, M. I., Huber, W. & Anders, S. Moderated estimation of fold change and dispersion for RNA-seq data with DESeq2. *Genome Biol.* **15**, 550 (2014).
94. Camacho, C. et al. BLAST+: architecture and applications. *BMC Bioinformatics* **10**, 421 (2009).
95. Verslues, P. E. & Bray, E. A. Role of abscisic acid (ABA) and *Arabidopsis thaliana* ABA-insensitive loci in low water potential-induced ABA and proline accumulation. *J. Exp. Bot.* **57**, 201–212 (2006).
96. Patro, R., Duggal, G., Love, M. I., Irizarry, R. A. & Kingsford, C. Salmon provides fast and bias-aware quantification of transcript expression. *Nat. Methods* **14**, 417–419 (2017).
97. Wu, T. et al. clusterProfiler 4.0: A universal enrichment tool for interpreting omics data. *Innovation* **2**, 100141 (2021).
98. Oksanen, J. et al. vegan: Community Ecology Package, R package version (2013).
99. de Mendiburu, F., de Mendiburu, M. F. Package 'agricolae'. *R Package, version 1*, (2019).
100. Liu, C., Cui, Y., Li, X. & Yao, M. microeco: an R package for data mining in microbial community ecology. *FEMS Microbiol. Ecol.* **97**, (2020).
101. Wen, T. et al. ggClusterNet: An R package for microbiome network analysis and modularity-based multiple network layouts. *iMeta* **1**, e32 (2022).
102. Csárdi, G. & Nepusz, T. The igraph software package for complex network research. *Inter J. Complex Syst.* **1965**, 1–9 (2006).
103. Agler, M. T. et al. Microbial hub taxa link host and abiotic factors to plant microbiome variation. *PLOS Biol.* **14**, e1002352 (2016).
104. Bastian, M., Heymann, S. & Jacomy, M. Gephi: an open source software for exploring and manipulating networks. *Proc. Int. AAAI Conf. Web Soc. media* **3**, 361–362 (2009).
105. Fick, S. E. & Hijmans, R. J. WorldClim 2: New 1-km spatial resolution climate surfaces for global land areas. *Int. J. Climatol.* **37**, 4302–4315 (2017).
106. Wickham, H. ggplot2: Elegant Graphics for Data Analysis (Springer, 2016).

Acknowledgements

We thank Dr. Cara Haney for the helpful discussion of the manuscript. We thank Dr. Xiang Liu for the helpful discussion of community assembly processes. We thank Drs. Yichuan Wang and Hongwei Guo for sharing root hair-related mutants. We are grateful for Drs. Yajun Chen, Wenjun Zhou (Xishuangbanna Tropical Botanic Garden(XTBG), Chinese Academy of Science), Guojing Wen, Daxin Yang (Yuanjiang Savanna Ecosystem Research Station, XTBG) and Tengxiang Lian (South China Agricultural University) for the collection of nature soil. We thank Dr. Jianbo Yang (Kunming Institute of Botany, Chinese Academy of Science) for making the ArcGIS images of the natural soil sample sites. The project was supported by the Stable Support Plan Program of Shenzhen Natural Science Fund Grant (20220815160107001), the NSFC General Project (32270286), and Shenzhen Science and Technology Program (Grant No. RCYX20231211090408015 and ZDSYS20230626091659010).

Author contributions

Y.S. and Z.W. developed the ideas and designed the project. Z.W., Z.L., and Y.Z. conducted experiments with the help of J.L., J. Z., X. T., Z.W., K.

G., and P.M. analyzed data. T.D. provided assistance in bacterial gene knock-out. Y.S. and Z.W. wrote the manuscript.

Competing interests

The authors declare no competing interests.

Additional information

Supplementary information The online version contains supplementary material available at <https://doi.org/10.1038/s41467-024-54417-5>.

Correspondence and requests for materials should be addressed to Yi Song.

Peer review information *Nature Communications* thanks Jessica Prenni, and the other anonymous reviewer(s) for their contribution to the peer review of this work. A peer review file is available.

Reprints and permissions information is available at <http://www.nature.com/reprints>

Publisher's note Springer Nature remains neutral with regard to jurisdictional claims in published maps and institutional affiliations.

Open Access This article is licensed under a Creative Commons Attribution-NonCommercial-NoDerivatives 4.0 International License, which permits any non-commercial use, sharing, distribution and reproduction in any medium or format, as long as you give appropriate credit to the original author(s) and the source, provide a link to the Creative Commons licence, and indicate if you modified the licensed material. You do not have permission under this licence to share adapted material derived from this article or parts of it. The images or other third party material in this article are included in the article's Creative Commons licence, unless indicated otherwise in a credit line to the material. If material is not included in the article's Creative Commons licence and your intended use is not permitted by statutory regulation or exceeds the permitted use, you will need to obtain permission directly from the copyright holder. To view a copy of this licence, visit <http://creativecommons.org/licenses/by-nc-nd/4.0/>.

© The Author(s) 2024